Lecture Note on

" Critical Phenomena from the Fuzzy Sphere Regularization"

W. Zhu[1]

[1] *Westlake Institute of Advanced Study,*

Westlake University, Hangzhou, P. C. China

CONTENTS

Critical phenomena near phase transitions constitute a cornerstone of modern physics with profound implications across condensed matter physics, statistical mechanics, quantum field theory (QFT) and quantum gravity [1–5]. Continuous transitions and related critical phenomena exhibit a remarkable property of universality, generally characterized by a set of critical exponents that describe non-analytic behavior of physical observables near critical points. For example, the liquid-gas transition shares the same universality class as the three-dimensional Ising magnetic transition. Universality offers extensive applications of the Ising model and general theories of critical phenomena, reaching fields such as pure mathematics, biology, earth science, deep learning, economics, just to name a few.

Regarding the field theory description of critical phenomena, distinct universality classes correspond to distinct renormalization group (RG) fixed points [1, 5, 6]. Remarkably, at these RG fixed points, the usual Poincaré symmetry (comprising Lorentz and translation symmetries) and scale invariance often enhance into a larger spacetime symmetry—conformal symmetry—first explicitly uncovered by Polyakov through the exact solution of the two-dimensional Ising transition [7]. Conformal symmetry preserves angles but not necessarily distances, signifying invariance under non-uniform RG transformations. Beyond its elegance, conformal symmetry has proven instrumental in solving critical phenomena. In two dimensions, conformal symmetry becomes infinite-dimensional [8], rendering numerous theories exactly solvable and thus giving birth to conformal field theory (CFT) [9], which significantly impacts diverse areas from condensed matter physics to quantum gravity. In higher dimensions (e.g., 3D), conformal symmetry is less restrictive, yet modern developments such as the conformal bootstrap method [10–12] have demonstrated that it remains highly effective for numerically determining precise critical exponents.

Despite widespread recognition of conformal symmetry's significance, its explicit application in studies of critical phenomena at three and higher dimensions, particularly in lattice models like the Ising model, remains limited [13–16]. This is primarily because lattice models typically employ torus geometries, where the implications of conformal symmetry are unclear, thus relying solely on scaling symmetry (finite-size scaling) to extract critical exponents. Conformal symmetry, however, becomes explicit on geometries like the sphere S^d or cylinder $S^{d-1} \times R$. On the cylinder, CFTs exhibit the state-operator correspondence (radial quantization) [17, 18], implying that quantum Hamiltonians defined on S^{d-1} have eigenstates directly corresponding to scaling operators of the infrared (IR) CFT. The energy

gaps of these eigenstates are proportional to the scaling dimensions of the respective operators, providing a powerful framework to investigate scaling dimensions, operator product expansion (OPE) coefficients, and operator algebras. In two dimensions, studying quantum lattice models on a one-dimensional periodic chain (S^1) naturally leverages this geometry [19–22], but in higher dimensions, curvature poses significant challenges for conventional lattice approaches [23, 24].

Remarkably, fuzzy sphere regularization has proven highly successful for understanding three-dimensional CFTs. Key achievements include: i) directly demonstrating conformal symmetry in the 3D Ising transition [25], the $O(N)$ Wilson-Fisher model [26, 27], and the $SO(5)$ deconfined phase transition [28] via state-operator correspondence; ii accurately computing crucial quantities such as OPE coefficients [29], four-point correlator [30] and the RG monotonic F-function [31]; iii) thoroughly exploring conformal line defects [32, 33] and boundaries [34, 35] in the 3D Ising transition; and iv) discovering new 3D CFTs related to Chern-Simons-matter theories [36]. These advances were facilitated the explicit conformal symmetry on spherical geometry, and by remarkably small finite-size effects, enabling computations that previously required millions of CPU hours to now be executed efficiently on standard laptops within an hour. While many exciting results are forthcoming, this review paper highlights significant progress already achieved.

I. MOTIVATION FROM THE CONFORMAL FIELD THEORY

A. Conformal transformation

Thus, we have four kinds of transformations:

- translation: $\epsilon_\mu = a_\mu$, i.e. ordinary translations independent of x.
- rotaion: $\epsilon_\mu = \omega_{\mu\nu} x_\nu$
- dilatation: $\epsilon_\mu = \lambda x_\mu$
- special conformal transformation: $\epsilon_\mu = b_\mu x^2 - 2x_\mu b_\nu x_\nu$

Locally, the above conformal transformation can be expressed as the conformal generators: $a_\mu \partial_\mu, \omega^\mu_\nu x^\nu \partial_\mu x_\mu, \lambda x \cdot \partial, b^\mu(x^2\partial_\mu - 2x^\mu x \cdot \partial)$, where the number of them are respec-

tively $d, d(d-1)/2, 1, d$. Thus, the total number generators for conformal symmetry is $(d+1)(d+2)/2$.

The generators are

$$P_\mu = -i\partial_\mu, \tag{1}$$

$$L_{\mu\nu} = i(x_\mu\partial_\nu - x_\nu\partial_\mu), \tag{2}$$

$$D = -ix_\mu\partial_\mu, \tag{3}$$

$$K_\mu = -i(2x_\mu x^\nu\partial_\nu - x^2\partial_\mu) \tag{4}$$

and they satisfy the commutation relations:

$$[D, P_\mu] = iP_\mu, \tag{5}$$

$$[D, K_\mu] = -iK_\mu, \tag{6}$$

$$[P_\rho, L_{\mu\nu}] = i(\eta_{\mu\nu}P_\nu - \eta_{\rho\nu}P_\mu), \tag{7}$$

$$... \tag{8}$$

Up to now, we consider the conformal transformation on the coordinates only. Here we consider how a quantum field changes under a given conformal transformation T_a: $\phi(x) \to \phi'(x') = (1 - i\epsilon_a T_a)\phi(x)$.

To understand the physics of above commutation relation, we make an anglog with the simple harmonics in quantum mechanics. That is, we think about dilatation operator D as Hamiltonian H in simple harmonics, translation operator P_μ (SCT operator K_μ) as rising ladder operator a^+ (lowering ladder operator a), then we get some similarity between CFT algebra and simple harmonics.

Then we define the CFT state $|\phi\rangle$ as the eigenstate of dilatation operator

$$D|\phi\rangle = \Delta_\phi|\phi\rangle \tag{9}$$

we immediately know that the eigenvalues of dilatation operator form the tower structure:

$$DP_\mu|\phi\rangle = (\Delta_\phi + 1)P_\mu|\phi\rangle \tag{10}$$

$$DK_\mu|\phi\rangle = (\Delta_\phi - 1)K_\mu|\phi\rangle \tag{11}$$

We call $P_\mu|\phi\rangle$ as the descendant field of $|\phi\rangle$. If $K_\mu|\phi\rangle = 0$, we call $|\phi\rangle$ as the *primary* field.

Simple harmonics problem.— Let us consider the hamiltonian

$$H = \frac{1}{2m}\nabla^2 + \frac{1}{2}m\omega^2 x^2 \tag{12}$$

By introducing the ladder operators,

$$a^+ = \sqrt{\frac{m\omega}{2}}x - i\frac{p}{\sqrt{2m\omega}}, a = \sqrt{\frac{m\omega}{2}}x + i\frac{p}{\sqrt{2m\omega}} \tag{13}$$

the hamiltonian becomes

$$H = \hbar\omega(a^+ a + \frac{1}{2}), \tag{14}$$

$$[H, a] = \hbar\omega[a^+ a, a] = -\hbar\omega a \tag{15}$$

$$[H, a^+] = \hbar\omega[a^+ a, a^+] = \hbar\omega a^+ \tag{16}$$

B. Constraints on correlation functions

The objects of interest in quantum field theories are n-point correlation functions which are usually computed in a perturbative approach via either canonical quantisation or the path integral method. In this section, we will see that the exact two- and three-point functions for certain fields in a conformal field theory are already determined by the symmetries. This will allow us to derive a general formula for the OPE among quasi-primary fields.

Now the 2-point function $G(z_1, z_2) = \langle\phi(z_1)\phi(z_2)\rangle$, under the scalse transformation $z \to \lambda z$,

$$\langle\phi(z_1)\phi(z_2)\rangle = \lambda^{2\Delta}\langle\phi(\lambda z_1)\phi(\lambda z_2)\rangle \tag{17}$$

Rotation and translation invariance require that

$$\langle\phi(z_1)\phi(z_2)\rangle = f(|z_1 - z_2|) \tag{18}$$

Inserting $f(|z_1 - z_2|)$ into the above equation leads to

$$\langle\phi(z_1)\phi(z_2)\rangle = f(|z_1 - z_2|) = \frac{C}{|z_1 - z_2|^{2\Delta}} \tag{19}$$

Similarly, for three-point correlator

$$\langle\phi_1(z_1)\phi_2(z_2)\phi_3(z_3)\rangle = \frac{f_{123}}{|z_1-z_2|^{\Delta_1+\Delta_2-\Delta_3}|z_2-z_3|^{\Delta_2+\Delta_3-\Delta_1}|z_3-z_1|^{\Delta_3+\Delta_1-\Delta_2}} \tag{20}$$

The scaling dimension Δ and Operator Product Expansion (OPE) coefficients are universal numbers, and they are the most important information for a given CFT. Using these data, one can reconstruct all critical phenomena near the phase transition.

Connection with the Critical Phenomena.— CFT is very useful in the statistical physics and condensed matter physics, especially in the phase transition and critical phenomena. A key feature of critical phenomena is the universality, where diverse physical systems exhibit identical scaling behaviors around phase transition point. It is rooted in the long wavelength effective field theory governing the critical phenomena. This section elucidates how the conformal data of CFT determine measurable critical exponents, bridging abstract field theory to microscopic observables [1, 3, 4].

In Landau-Ginzburg-Wilson theory, the free energy near a critical point is governed by local fields such as order parameter ϕ and energy density ϕ^2. These map to the relevant CFT primaries:

$$\begin{aligned}\phi(\text{local order parameter}) &\longleftrightarrow \sigma \text{ (lowest symmetry-odd primary)}\\ \phi^2(\text{energy density}) &\longleftrightarrow \epsilon \text{ (lowest symmetry-even primary).}\end{aligned} \tag{21}$$

Thus, the critical exponents relating to the local fields are solely determined by the scaling dimensions of CFT primaries. The widely used critical exponents $(\eta, \nu, \beta, \gamma, \delta)$ of Wilson-Fisher universality class relates to the scaling dimensions Δ_σ, Δ_ϵ as

$$\eta = 2\Delta_\sigma - (d-2), \tag{22}$$

$$\nu = \frac{1}{d-\Delta_\epsilon}, \tag{23}$$

$$\beta = \frac{\nu}{2}(d-2+\eta), \tag{24}$$

$$\gamma = \nu(2-\eta), \tag{25}$$

$$\delta = \frac{d+2-\eta}{d-2+\eta}. \tag{26}$$

Additionally, CFT also governs physics close to or around the exact critical point. For example, in the finite-size simulation on a given size L, the subleading correction to

the free energy reads:

$$F \sim L^{-d}\left(a_0 + a_1 L^{-\omega} + \cdots\right),$$

where anomalous critical exponent $\omega = \Delta_{\epsilon'} - d$ is determined by the lowest irrelevant symmetry-even primary ϵ'.

C. Radial quantization

To see the consequences of conformal invariance in a two dimensional quantum field theory, we enter into some of the details of the quantization procedure (we first take conformal field theories defined on Euclidean two-dimensional flat space.). We begin with flat Euclidean "space" and "time" coordinates σ and τ (In Minkowski space, one needs to make a Wick rotation $\tau = it$). The coordinate $\sigma = \sigma + 2\pi$, is the periodic boundary condition for 1d spatial dimension (Or, it is to eliminate any infrared divergences, we compactify the space coordinate). Thus, we define the complex number $\zeta = \tau + i\sigma$.

The conformal map

$$z = \exp(\tau + i\sigma) \tag{27}$$

maps the cylinder to the complex plane. Equal time surfaces, $\tau = const$, become circles of constant radius on the z-plane, and time reversal, $\tau \to -\tau$, becomes $z \to 1/z^*$. Then the time translation $\tau -> \tau + T$ becomes dilatation on the complex plane $z -> e^T z$. So the dilatation generator on the conformal plane can be regarded as the Hamiltonian for the system, and the Hilbert space is built up on surfaces of constant radius. This procedure for defining a quantum theory on the plane is known as radial quantization (Hilbert state space defined on circles about the origin, and propagation of states in the radial direction dilation operator is the Hamiltonian; rotation operator is a spatial translation). Thus the hamiltonian on the complex plane is

$$H \leftrightarrow D \tag{28}$$

The radial quantization, in particular, is to quantize this Hamiltonian or said to quantize the generators on the complex plane.

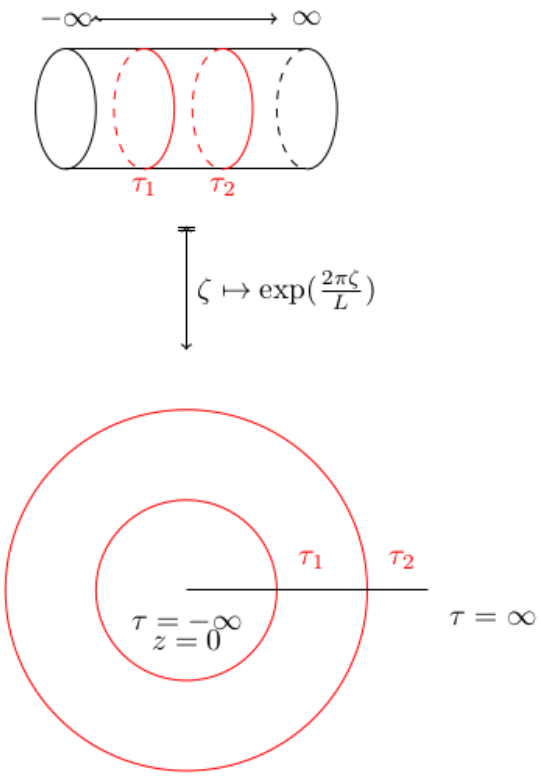

FIG. 1. Map from cylinder to plane in 2D.

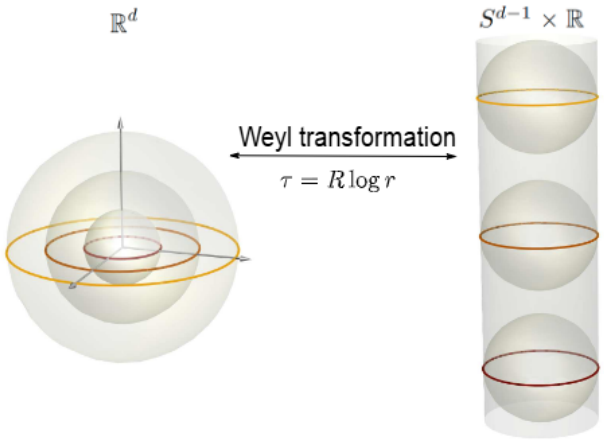

FIG. 2. Map from cylinder to plane in 3D.

Another way to view this relation is, under that map Eq. 27, the field changes as

$$\phi_{cyl}(\tau, \Omega) = \Lambda(r, \Omega)^{\Delta/2} \phi_{plane}(r, \Omega) \tag{29}$$

where $\Lambda = R^{-2} e^{\frac{2\tau}{R}}$ is the scale factor of this transformation and we can see it by considering

the metric

$$ds^2 = dr^2 + r^2 d\Omega^2 = R^{-2} e^{\frac{2\tau}{R}} \left(d\tau^2 + R^2 d\Omega^2 \right) = \Lambda(r, \Omega) \left(d\tau^2 + R^2 d\Omega^2 \right). \tag{30}$$

So we have

$$\langle \phi_{cyl}(\tau) \phi_{cyl}(0) \rangle = \Lambda(r, \Omega)^{\Delta/2} \Lambda(r = 1, \Omega)^{\Delta/2} \langle \phi_{plane}(\tau) \phi_{plane}(0) \rangle \tag{31}$$

$$= R^{-2} e^{\frac{\tau \Delta}{R}} R^{-2} \frac{1}{|r-1|^{2\Delta}} \sim e^{\frac{-\tau \Delta}{R}} \tag{32}$$

This is expontial decay function. Recalling that, the inverse of correlation length is proportional the eigenenergy gap, we have

$$\Delta E = E_n - E_0 \sim \frac{1}{\xi} = \frac{\Delta}{R} \tag{33}$$

So we reach the state-operator correspondence: *On the cylinder geometry $S^{d-1} \times R$, each eigenenergy gap has one-to-one correspondence with scaling dimension of CFT operator.* [17, 18].

Example.- Let us consider an example of 1+1D transverse Ising model, which develops 1+1D Ising CFT at the phase transition point.

$$H = \sum_n \sigma_n^z \sigma_{n+1}^z + h \sum_n \sigma_n^x \tag{34}$$

The duality ensures the transition occurs at $h_c = 1$. The periodic boundary condition leads to $S^1 \times R$ geometry. Plotting the energy spectra at the transition point will give Fig. 3.

Next we solve this model with periodic boundary condition. The stategy is to use the fermionic representative [Two-dimensional Ising model as a soluble problem of many fermions, T. D. Schultz, D. C. Mattis, E. H. Lieb]. Here we make the Jordan-Wigner transformation

$$c_n = \frac{\sigma_n^x + i\sigma_n^y}{2} \prod_{m<n} \sigma_m^z, c_n^\dagger = \frac{\sigma_n^x - i\sigma_n^y}{2} \prod_{m<n} \sigma_m^z, \tag{35}$$

$$\sigma_n^+ = \prod_{m<n} (1 - 2c_m^\dagger c_m) c_n, \sigma_n^- = \prod_{m<n} (1 - 2c_m^\dagger c_m) c_n^\dagger, \sigma_n^z = 1 - 2c_n^\dagger c_n \tag{36}$$

The string $\prod_{m<n}(1-2c_m^\dagger c_m)$ takes values ± 1, depending on even/odd number of fermions on the left side of n. One can check that,

$$\{c_n, c_m^\dagger\} = \delta_{m,n}, \{c_n, c_m\} = \{c_n^\dagger, c_m^\dagger\} = 0 \tag{37}$$

$$[\sigma_n^+, \sigma_m^-] = \delta_{n,m}\sigma_n^z, [\sigma_n^z, \sigma_m^\pm] = \pm 2\delta_{n,m}\sigma_n^\pm \tag{38}$$

(Only the Pauli matrix with the same site index should consider the commutation relation $\{\sigma_i^a, \sigma_j^b\} = 2\delta_{ij}\delta_{ab}, [\sigma_i^+, \sigma_j^-] = \delta_{ij}\sigma_j^z$.)

Under the Jordan-Wigner transformation, the Hamiltonian becomes

$$\begin{aligned} H &= \sum_n \sigma_n^z - \sum_n \sigma_n^x \sigma_{n+1}^x \\ &= \sum_{n=1}^{N}(1-2c_n^\dagger c_n) - \sum_{n=1}^{N-1}[c_n^\dagger c_{n+1}^\dagger + c_n^\dagger c_{n+1} + h.c.] + (c_N^\dagger c_1^\dagger + c_N^\dagger c_1 + h.c.)e^{i\pi\mathcal{N}}, \mathcal{N} = \sum_n c_n^\dagger c_n \end{aligned} \tag{39}$$

with

$$\begin{aligned} \sigma_n^x \sigma_{n+1}^x &= [\prod_{m<n}(1-2c_m^\dagger c_m)](c_m + c_m^\dagger)[\prod_{k<n+1}(1-2c_k^\dagger c_k)](c_k + c_k^\dagger) \\ &= (c_n^\dagger + c_n)(1-2c_n^\dagger c_n)(c_{n+1} + c_{n+1}^\dagger) \\ &= c_n^\dagger c_{n+1} + c_n^\dagger c_{n+1}^\dagger + h.c. \end{aligned} \tag{40}$$

The boundary term comes from that $\sigma_N^x \sigma_1^x = e^{i\pi\sum_{j<L} n_j} c_N^\dagger c_1 = -e^{i\pi\sum_{j\leq L} n_j} c_N^\dagger c_l = -e^{i\pi\mathcal{N}} c_N^\dagger c_l$, because to the left of $c_N^\dagger$ we certainly have $n_N = 1$. This shows that boundary condition are changed by fermion parity $e^{i\pi\mathcal{N}} = (-1)^{\mathcal{N}}$ and periodic boundary condition become anti-periodic boundary condition when $\mathcal{N}$ is even. And odd $\mathcal{N}$ relates to periodic boundary condition. Therefore, the real spin problem is not exactly the same with free fermion. Next, for odd $\mathcal{N}$, we set $e^{ikN} = 1, k = \frac{2\pi n}{N}, n = -N/2+1, ..., 0, ..., N/2$, for even $\mathcal{N}$, we set $e^{ikN} = -1, k = \pm\frac{\pi(2n-1)}{N}, n = 1, ..., N/2$.

In terms of momentum space $c_j = \frac{1}{\sqrt{N}} \sum_k e^{ikj} c_k$, the Hamiltonian becomes

$$\begin{aligned} H &= -\sum_k [2\cos(k) c_k^\dagger c_k + (e^{ik} c_k^\dagger c_{-k}^\dagger + h.c.)] + \sum_k (2c_k^\dagger c_k - 1) \\ &= \sum_k [(1-\cos(k))(c_k^\dagger c_k - c_{-k} c_{-k}^\dagger) - (e^{ik} c_k^\dagger c_{-k}^\dagger + h.c.)] \\ &= \sum_{k>0} [(1-\cos(k))(c_k^\dagger c_k - c_{-k} c_{-k}^\dagger) - (e^{ik} c_k^\dagger c_{-k}^\dagger + h.c.)] + \sum_{k<0} ... \\ &= \sum_{k>0} [2(1-\cos(k))(c_k^\dagger c_k - c_{-k} c_{-k}^\dagger) - (2i\sin(k) c_k^\dagger c_{-k}^\dagger - 2i\sin(k) c_{-k} c_k)] \\ &= \sum_{k>0} (c_k^\dagger, c_{-k}) \begin{pmatrix} 2(1-\cos(k)) & -2i\sin(k) \\ 2i\sin(k) & 2(1-\cos(k)) \end{pmatrix} \begin{pmatrix} c_k \\ c_{-k}^\dagger \end{pmatrix} \end{aligned} \tag{41}$$

where we used $\sum_k 2\cos(k) c_k^\dagger c_k = \sum_k \cos(k)(c_k^\dagger c_k - c_{-k} c_{-k}^\dagger)$, and $\sum_k (2c_k^\dagger c_k - 1) = \sum_k (c_k^\dagger c_k - c_{-k} c_{-k}^\dagger)$.

The diagonalization is akin to Bogovliubov transformation, and all eigenvalues can be calculated:

$$\Lambda(k) = \pm 2\sqrt{(\cos(k)-1)^2 + \sin^2(k)} = \pm 2\sin\frac{k}{2} \tag{42}$$

So we obtain that, for odd N, we have $e^{ikN} = 1, k = \frac{2\pi n}{N}, n = -N/2, ..., 0, ..., N/2$,

$$H = \sum_{n=0}^{N-1} \Lambda^-(n)(\eta_n^\dagger \eta_n - \frac{1}{2}) + const. \tag{43}$$

$$\Lambda^-(n) = [(1-\cos\frac{2\pi n}{N})^2 + (\sin\frac{2\pi n}{N})^2]^{1/2} = 2\sin\frac{2\pi n}{2N} \tag{44}$$

where Bogoliubov particle as $\begin{pmatrix} c_q \\ c_{-q}^\dagger \end{pmatrix} = \begin{pmatrix} u_q & -iv_q \\ -iv_q & u_q \end{pmatrix} \begin{pmatrix} \eta_q \\ \eta_{-q}^\dagger \end{pmatrix}$. (We have used that $H = \sum_{k>0} \Lambda(k)(\eta_k^\dagger \eta_k + \eta_{-k} \eta_{-k}^\dagger) = \sum_k \Lambda(k)(\eta_k^\dagger \eta_k - 1/2)$) For even N, we know the boundary condition is $e^{ikN} = -1, k = \pm\frac{\pi(2n-1)}{N}, n = 1, ..., N/2$.

$$H = \sum_{n=1}^{N/2} \Lambda^+(n)(\eta_n^\dagger \eta_n - \frac{1}{2}) + const. \tag{45}$$

$$\Lambda^+(n) = [(1-\cos\frac{\pi(2n-1)}{N})^2 + (\sin\frac{\pi(2n-1)}{N})^2]^{1/2} = 2\sin\frac{\pi(2n-1)}{2N} \tag{46}$$

The expression for H in above allows to immediately conclude that the ground state of the Hamiltonian must be the Bogoliubov vacuum state $|0\rangle$ which annihilates the

$\vec{\eta}_k|0\rangle = 0$ for all k. Thus, the ground state energy is

$$E_0^+ = -\frac{1}{2}\sum_{n=1}^{N/2}\Lambda^+(n) + const. = -csc\frac{\pi}{2N} + const \approx -\frac{2N}{\pi} - \frac{\pi}{12N} + ... \tag{47}$$

$$E_0^- = -\frac{1}{2}\sum_{n=1}^{N/2-1}\Lambda^-(n) + const. = -cot\frac{\pi}{2N} + const \approx -\frac{2N}{\pi} + \frac{\pi}{6N} + ... = E_0^+ + \frac{\pi}{4N} \tag{48}$$

The lowest excited energy in even sector is

$$E_1^+ = \Lambda^+(1) + \Lambda^+(N/2) + E_0^+ = 4\sin\frac{\pi}{2N} + E_0^+ \approx \frac{2\pi}{N} + E_0^+ \tag{49}$$

Finally, according to the CFT, we have

$$H = \frac{1}{2\pi}\int_0^N dy[T'(w) + \bar{T}'(\bar{w})] = \frac{2\pi}{N}(L_0 + \bar{L}_0) - \frac{\pi c}{6N} + K \tag{50}$$

where K is a constant. Then we use the state $|\Delta\rangle$, $L_0|\Delta{+}n\rangle = (\Delta{+}n)|\Delta{+}n\rangle, \bar{L}_0|\bar{\Delta}{+}n\rangle = (\bar{\Delta}+n)|\bar{\Delta}+n\rangle$. We got the eigenvalues as

$$E = \frac{2\pi}{N}(\Delta + \bar{\Delta} + n + \bar{n}) - \frac{\pi c}{6N} + K, \tag{51}$$

$$E_0 = -\frac{\pi c}{6N} + K \tag{52}$$

Compare E_0^+ ($1/N$ term) with CFT result, we have $c = 1/2$. And we used $csc(x) \approx \frac{1}{x} + \frac{x}{6} + .., cot(x) \approx \frac{1}{x} - \frac{x}{3} + ..$

Comparing E_1^+ with CFT, we have

$$\Delta_\epsilon = \bar{\Delta}_\epsilon = 1/2 \tag{53}$$

Comparing E_0^- with CFT

$$\Delta_\sigma = \bar{\Delta}_\sigma = 1/16 \tag{54}$$

In conclusion, the state-operator correspondence works in 2D Ising transition.

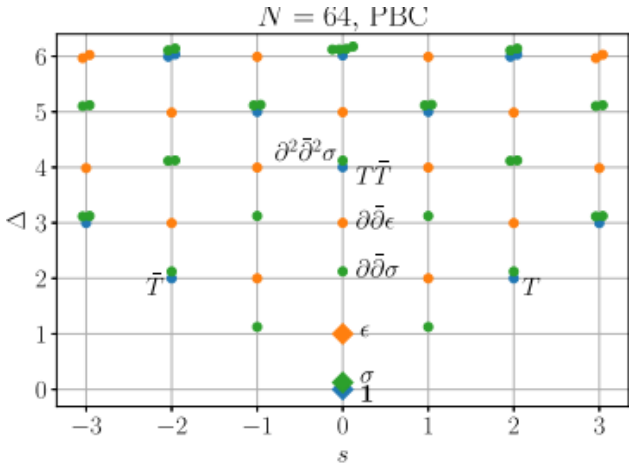

FIG. 3. Operator spectra of 1+1 transverse Ising model at the transition point.

II. LANDAU LEVELS ON THE SPHERE GEOMETRY

In the Haldane's spherical geometry, the two-dimensional sheet containing electrons is wrapped around the surface of a sphere, and a perpendicular magnetic field is generated by placing a Dirac magnetic monopole at the center of the sphere. The spherical geometry is compact, i.e. it does not have edges, which makes it suitable for an investigation of the bulk properties. In particular, filled Landau levels are unambiguously defined. The spherical geometry has been instrumental in establishing the validity of the theory of the FQHE, and provides the cleanest proofs for many properties, which was first introduced by Haldane [37].

A. Landau levels on sphere

We consider a sphere of radius R and put a monopole charge $2s_0$ at its center. The monopole generates a magnetic field $\mathbf{B}$ extending radially outward through the surface. $2s_0$ must be an integer due to Dirac's monopole quantization condition. The flux corresponds to a magnetic field

$$\mathbf{B} = \frac{2s_0\phi_0}{4\pi R^2}\hat{r} \tag{55}$$

which and is produced by the vector potential

$$\mathbf{A} = -\frac{2s_0\phi_0}{4\pi R}\cot\theta\vec{\phi}, \tag{56}$$

$$\nabla\times\mathbf{A} = \frac{1}{r\sin\theta}[\frac{\partial}{\partial\theta}(A_\phi\sin\theta) - \frac{\partial}{\partial\phi}A_\theta]\vec{r} + \frac{1}{r}[\frac{1}{\sin\theta}\frac{\partial}{\partial\phi}A_r - \frac{\partial}{\partial r}(rA_\phi)]\vec{\theta} + \frac{1}{r}[\frac{\partial}{\partial r}(rA_\theta) - \frac{\partial}{\partial\theta}A_r]\vec{\phi} \tag{57}$$

The kinetic energy operator is given by

$$H_0 = \frac{\hbar^2}{2mR^2}|\mathbf{\Lambda}|^2 \tag{58}$$

where the canonical momentum is defined as (by setting $\hbar \equiv 1$)

$$\begin{aligned}\mathbf{\Lambda} &= R\vec{r}\times(-i\nabla + e\mathbf{A}) \\ &= R\vec{r}\times[-i(\vec{\theta}\frac{\partial}{\partial\theta}\vec{\phi}\frac{1}{\sin\theta}\frac{\partial}{\partial\phi}) - s_0\cot\theta\vec{\phi}] = -i[\vec{\phi}\frac{\partial}{\partial\theta} - \vec{\theta}\frac{1}{\sin\theta}\frac{\partial}{\partial\phi}] + s_0\cot\theta\vec{\theta}\end{aligned} \tag{59}$$

where we used $\vec{r}\times\vec{\theta} = \vec{\phi}, \vec{r}\times\vec{\phi} = -\vec{\theta}$, and $\nabla = \vec{r}\frac{\partial}{\partial r} + \vec{\theta}\frac{\partial}{r\partial\theta} + \vec{\phi}\frac{\partial}{r\sin\theta\partial\phi}$.

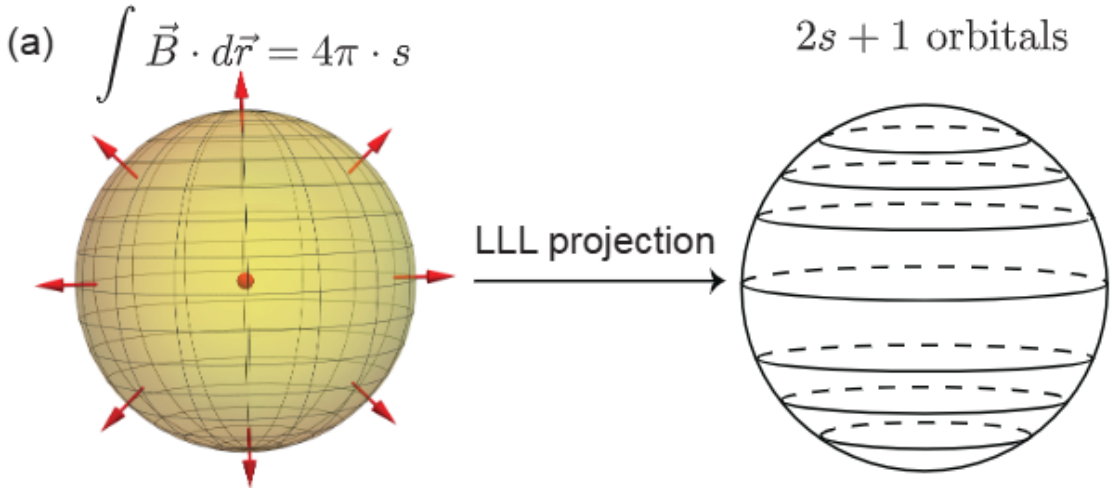

FIG. 4. Schematic plot of electrons moving on a sphere in the presence of $4\pi \cdot s$ monopole. The LLL has $2s+1$ degenerate orbitals, which form an $SO(3)$ spin-s irreducible representation. A system projected into the LLL can be equivalently viewed as a fuzzy sphere.

Using the Levi-Civita symbol to rewrite

$$\Lambda_i = M_i + e\epsilon_{ijk} r_j A_k = -i\hbar\epsilon_{ijk} r_j \partial_k + e\epsilon_{ijk} r_j A_k \tag{60}$$

where M_i is the canonical angular momentum and satisfy $[M_i, M_j] = i\hbar\epsilon_{ijk} M_k$. The commutator of Λ are

$$\begin{aligned}
[\Lambda_i, \Lambda_j] &= [M_i, M_j] + e\epsilon_{jcd}[M_i, r_c A_d] - e\epsilon_{iab}[M_i, r_a A_b] \\
&= i\hbar\epsilon_{ijk} M_k + ie\hbar\epsilon_{iba}\epsilon_{jca}(r_b A_c - r_c A_b) + ie\hbar\epsilon_{iab}\epsilon_{jcd}(\partial_d A_b - \partial_b A_d) \\
&= i\hbar\epsilon_{ijk} M_k + ie\hbar\epsilon_{ijk}(\mathbf{r} \times \mathbf{A})_k + ie\hbar\epsilon_{iab}\epsilon_{jcd}\epsilon_{dbe} r_a r_b B_e \\
&= i\hbar\epsilon_{ijk}(\Lambda_k - \hbar s_0 \Omega_k)
\end{aligned} \tag{61}$$

Similarly, we have

$$[\Lambda_i, \vec{r}_j] = [M_i, r_j/R] = i\epsilon_{ijk}\vec{r}_k \tag{62}$$

Finally, we can define the operator L_i as

$$\mathbf{L} = \mathbf{\Lambda} + s_0 \vec{r} \tag{63}$$

This operator forms su(2) algebra

$$[L_i, L_j] = i\varepsilon_{ijk} L_k \tag{64}$$

So the operator $\mathbf{L}^2$ should be quantized with eigenvalues $s(s+1)$, $2s \in Z$.

Using $\mathbf{\Lambda} \cdot \vec{r} = 0$, we have

$$|\mathbf{\Lambda}|^2 = L^2 - s_0^2 \tag{65}$$

The Hamiltonian, therefore, commutes with the angular momentum operators. Because $[L^2, L_z] = 0$, we choose eigenfunctions that simultaneously diagonalize $H, \hat{L}^2, \hat{L}_z$. These eigenfunctions are called "monopole harmonics", denoted by $Y_{s,m}^{(2s_0)}$.

$$\hat{L}^2 Y_{s,m}^{(s_0)} = s(s+1) Y_{s,m}^{(s_0)}, \tag{66}$$

$$\hat{L}_z Y_{s,m}^{(s_0)} = m Y_{s,m}^{(s_0)} \tag{67}$$

The eigenvalues of $|\Lambda|^2$ are $s(s+1) - s_0^2$, giving the energy eigenvalues

$$E_{s_0,l,m} = \frac{\hbar^2}{2mR^2}[s(s+1) - s_0^2] = \hbar\omega_c \frac{s(s+1) - s_0^2}{2|s_0|} \tag{68}$$

$$= \hbar\omega_c [n + \frac{1}{2} + \frac{n(n+1)}{2|s_0|}] \tag{69}$$

where we used $2s_0\phi_0 = 4\pi R^2 B$, and $s = s_0 + n$ (n hence labels the Landau levels).

Next we proceed to obtain the explicit expression for the single particle eigenstate, $Y_{s,m}^{(s_0)}$. A complete, orthogonal basis of the states spanning the lowest Landau level ($n = 0, s = s_0$) is given by

$$\psi_m^s(u, v) = u^{s+m} v^{s-m}, \tag{70}$$

$$u = \cos\frac{\theta}{2} e^{i\phi/2}, v = \sin\frac{\theta}{2} e^{-i\phi/2} \tag{71}$$

with $m = -s, -s+1, ..., s$. And we obtain the monopole harmonics functions

$$Y_{s,m}^{(s_0)} \stackrel{!}{=} [\frac{(2s+1)!}{4\pi(s-m)!(s+m)!}]^{1/2} v^{s-m} u^{s+m} \tag{72}$$

B. Landau level projection

The Landau levels are gapped spectrum. The finite energy gap is very important. Due the appearance of this energy gap, we can project out the higher energy levels, and project into the lowest Landau level (LLL) subspace. We can construct effective theory based on the LLL. This technique has been widely used in the study of the fractional quantum Hall effect, which is belong to the gapped topological order.

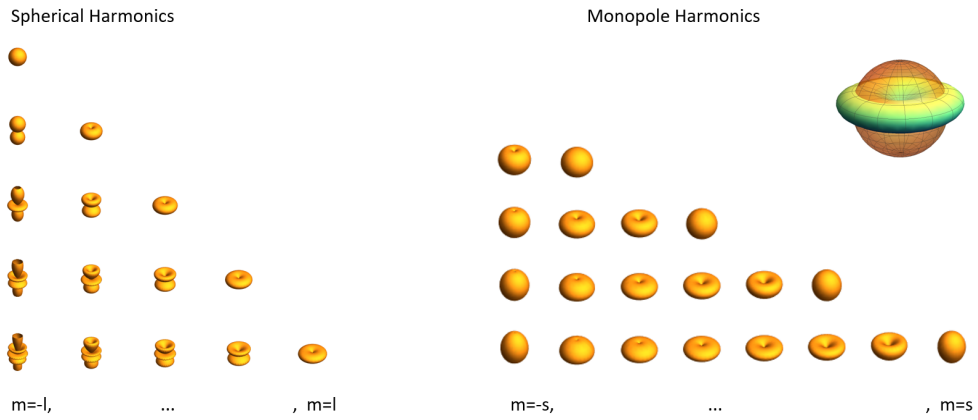

FIG. 5. Monopole harmonics.

It is worth noting that this LLL projection is controlled, because the kinetic energy is quenched. Say, generally the projection is controlled under the condition of $W \ll U \ll \Delta$, where W is the bandwidth of projected band, U is the interaction strength of particles and Δ is the energy band gap separating the projected energy band from the higher energy bands. In traditional condensed matter systems, this condition is usually violates because W is generally nonzero. Fortunately, W is exactly zero in the Landau level problem, so the condition of $W \ll U \ll \Delta$ can be easily satisfied by tuning the interaction strength. And, importantly, no matter how small U is, this problem is strongly-correlated (since kinetic energy is quenched). In a word, this LLL projection is always controlled and we can apply it safely.

The great advantage of the LLL enormously simplifies computer experimentation; the dimension of the relevant Fock space is finite because of the LLL constraint, allowing us to obtain exact results. This idea is similar to the "regularization" in the field theory.

At last, the LLL on the sphere indeed corresponds to the fuzzy sphere, a fundamental example of non-commutative geometry in mathematics. To provide an intuitive understanding of the emergence of the fuzzy sphere, we consider the projection of the coordinates of a unit sphere, denoted as $\vec{x} = (\sin\theta\cos\varphi, \sin\theta\sin\varphi, \cos\theta)$. After the projection, these coordinates become three $(2s+1) \times (2s+1)$ matrices, given by

$$(\vec{X})_{m_1,m_2} = \int \sin\theta \, \mathrm{d}\theta \, \mathrm{d}\varphi \, \vec{x} \, \bar{Y}^{(s)}_{s,m_1}(\theta,\varphi) Y^{(s)}_{s,m_2}(\theta,\varphi). \tag{73}$$

These matrices satisfy the following commutation relations:

$$[\mathbf{X}^\mu, \mathbf{X}^\nu] = \frac{1}{s+1} i\epsilon^{\mu\nu\rho}\mathbf{X}_\rho. \tag{74}$$

The fact that the three projected coordinates satisfy the SO(3) algebra formally defines a fuzzy sphere [38]. Notably, in the limit $s \to \infty$, the fuzziness disappears, and the commutative unit sphere is recovered. This limit also corresponds to the continuum limit in our fuzzy sphere regularization.

C. Second quantization using monopole harmonics

We consider the interacting field theory

$$H = \frac{1}{2}\int d\mathbf{r}d\mathbf{r}'\bar{\psi}(\mathbf{r})\bar{\psi}(\mathbf{r}')V(r-r')\psi(\mathbf{r}')\psi(\mathbf{r}) \tag{75}$$

where $V(r-r')$ is the interaction scattering potential.

Using the monopole harmonics, we introduce the second quantization scheme as

$$\hat{\psi}(\theta,\varphi) = \sum_{m=-s}^{s} \overline{Y}_{s,m}^{(s_0)}(\theta,\varphi)\hat{c}_m. \tag{76}$$

We can write down the second quantization form of hamiltonian with two-body interaction

$$H = \frac{1}{2}\sum_{m_1,m_2,m_3,m_4=-s}^{s} c_{m_1,n}^{\dagger}c_{m_2,n}^{\dagger}c_{m_3,n}c_{m_4,n}\delta_{m_1+m_2,m_3+m_4}\langle s,m_1;s,m_2|V|s,m_3;s,m_4\rangle \tag{77}$$

where the n is Landau level index and $s = s_0 + n$ is orbital momentum (s_0 is the magnetic monopole placed in the center of sphere). Next we consider the lowest Landau level with $n = 0$ case. The matrix element is

$$\langle s,m_1;s,m_2|V|s,m_3;s,m_4\rangle = \int d\Omega_1 \int d\Omega_2 \overline{Y}_{s,m_1}^{(s_0)}(\mathbf{r}_1)\overline{Y}_{s,m_2}^{(s_0)}(\mathbf{r}_2)V(\mathbf{r}_1,\mathbf{r}_2)Y_{s,m_3}^{(s_0)}(\mathbf{r}_2)Y_{s,m_4}^{(s_0)}(\mathbf{r}_1) \tag{78}$$

where $Y_{s,m}^{(s_0)}(\mathbf{r})$ is monopole harmonics functions.

If the potential V is a function of $|\mathbf{r}_1 - \mathbf{r}_2|$ (as is the case for the Coulomb potential), it can expanded in Legendre polynomials,

$$V(|\mathbf{r}_1 - \mathbf{r}_2|) = \sum_{k=0}^{\infty} U_k(\mathbf{r}_1,\mathbf{r}_2)P_k(\cos\theta_{12}) \tag{79}$$

and

$$U_k = \frac{1}{2}\int_0^{\pi} d\theta V(r_{12})P_k(\cos\theta)\sin\theta. \tag{80}$$

So the interaction can be rewritten in terms of a new set of parameters, U_k. The U_k are unitless coefficients that defines the potential. Let us show several examples here:

- For coulomb potential $V(r) = \frac{1}{r}$, we define the chord distance between two points on a sphere is given by

$$V(r) = V(|\mathbf{r}_1 - \mathbf{r}_2|) = \frac{1}{2R|\sin\frac{\theta_1-\theta_2}{2}|} = \frac{1}{R\sqrt{2-2\cos\theta_{12}}} = \frac{1}{R}\sum_n P_n(\cos\theta_{12}) \quad (81)$$

, where we need the formula for Legendre polynomials $P_n(x)$:

$$\frac{1}{\sqrt{1-2xt+t^2}} = \sum_{n=0} P_n(x)t^n. \quad (82)$$

So we have $U_k = 1$.

- For short-ranged potential $V(r) = \delta(\mathbf{r})$, we can use the expansion

$$\delta(\Omega_a - \Omega_b) = \sum_{l=0}^{\infty}\sum_{m=-l}^{l} Y^*_{l,m}(\Omega_a)Y_{l,m}(\Omega_b) = \sum_{l=0}^{\infty}(2l+1)P_l(\cos\theta_{ab}) \quad (83)$$

, where we used $P_l(\cos\theta_{ab}) = \frac{4\pi}{2l+1}\sum_{m=-l}^{l} Y^*_{lm}(\Omega_a)Y_{lm}(\Omega_b)$ (Y_{lm} is sphere harmonics function). Thus we have $U_k = 2k+1$ for short-ranged potentials.

- For short-ranged potential $V(r) = \nabla^2\delta(\mathbf{r})$, we use the expansion

$$\nabla^2_a\delta(\Omega_a - \Omega_b) = \sum_{l=0}^{\infty}\sum_{m=-l}^{l} \nabla^2_a Y^*_{l,m}(\Omega_a)Y_{l,m}(\Omega_b) = \sum_{l=0}^{\infty}\sum_{m=-l}^{l}(-l(l+1))Y^*_{l,m}(\Omega_a)Y_{l,m}(\Omega_b) = \sum_{l=0}^{\infty}(-l(l+1)$$

(84)

, where we used $P_l(\cos\theta_{ab}) = \frac{4\pi}{2l+1}\sum_{m=-l}^{l} Y^*_{lm}(\Omega_a)Y_{lm}(\Omega_b)$ (Y_{lm} is sphere harmonics function). Thus we have $U_k = -k(k+1)(2k+1)$ for short-ranged potentials.

Next we insert the potential form Eq. 79 into the matrix element, we have

$$\langle s, m_1; s, m_2|V|s, m_3; s, m_4\rangle = \int d\Omega_1 \int d\Omega_2 \overline{Y}^{(s_0)}_{s,m_1}(\mathbf{r}_1)\overline{Y}^{(s_0)}_{s,m_2}(\mathbf{r}_2)V(\mathbf{r}_1,\mathbf{r}_2)Y^{(s_0)}_{s,m_3}(\mathbf{r}_2)Y^{(s_0)}_{s,m_4}(\mathbf{r}_1)$$

$$= \int d\Omega_1 \int d\Omega_2 \overline{Y}^{(s_0)}_{s,m_1}(\Omega_1)\overline{Y}^{(s_0)}_{s,m_2}(\Omega_2)[\sum_k U_k \frac{4\pi}{2k+1}\sum_{m=-k}^{k} Y^*_{km}(\Omega_1)Y_{km}(\Omega_2)]Y^{(s_0)}_{s,m_3}(\Omega_2)Y^{(s_0)}_{s,m_4}(\Omega_1)$$

$$= \sum_k U_k \frac{4\pi}{2k+1}\sum_{m=-k}^{k} \times \int d\Omega_1 \overline{Y}^{(s_0)}_{s,m_1}(\Omega_1)\overline{Y}_{km}(\Omega_1)Y^{(s_0)}_{s,m_4}(\Omega_1)\int d\Omega_2 \overline{Y}^{(s_0)}_{s,m_2}(\Omega_2)Y_{km}(\Omega_2)Y^{(s_0)}_{s,m_3}(\Omega_2)$$

(85)

To deal with this integral, we explicitly substitute the monopole harmonic with $s_0 = 0$ for the spherical harmonics: $Y_{lm} = Y_{lm}^{s_0=0}$. Then we use the result from Ref. [39]:

$$\int d\Omega Y_{s_1,m_1}^{(Q_1)}(\Omega) Y_{s_2,m_2}^{(Q_2)}(\Omega) Y_{s_3,m_3}^{(Q_3)}(\Omega) =$$
$$(-)^{s_1+s_2+s_3}[\frac{(2s_1+1)(2s_2+1)(2s_3+1)}{4\pi}]^{1/2} \begin{pmatrix} s_1 & s_2 & s_3 \\ m_1 & m_2 & m_3 \end{pmatrix} \begin{pmatrix} s_1 & s_2 & s_3 \\ Q_1 & Q_2 & Q_3 \end{pmatrix} \quad (86)$$

where the round brackets are 3j symbols, and it is nonzero only if $Q_1 + Q_2 + Q_3 = 0$ and $m_1 + m_2 + m_3 = 0$. And the relation is also need: $\overline{Y}_{l,m}^{s_0} = (-)^{s_0+m} Y_{l,-m}^{-s_0}$.

Under this useful integrals, we can integrate over the angular coordinates $\Omega_{1,2}$, and we reach

$$H = \frac{1}{2} \sum_{m_1,m_2,m_3,m_4=-s}^{s} c_{m_1,n}^\dagger c_{m_2,n}^\dagger c_{m_3,n} c_{m_4,n} \delta_{m_1+m_2,m_3+m_4} \langle s, m_1; s, m_2 | V | s, m_3; s, m_4 \rangle$$
$$\langle s, m_1; s, m_2 | V | s, m_3; s, m_4 \rangle = \sum_{k=0}^{k_{max}} U_k (-)^{2s_0+m_2+m_4+4s+2k} [(2s+1)]^2 \times$$
$$\begin{pmatrix} s & k & s \\ -m_1 & m_1 - m_4 & m_4 \end{pmatrix} \begin{pmatrix} s & k & s \\ -m_2 & m_2 - m_3 & m_3 \end{pmatrix} \begin{pmatrix} s & k & s \\ -s_0 & 0 & s_0 \end{pmatrix} \begin{pmatrix} s & k & s \\ -s_0 & 0 & s_0 \end{pmatrix} \quad (87)$$

Here, for a general Wigner 3j coefficient, $\begin{pmatrix} s_1 & s_2 & s_3 \\ m_1 & m_2 & m_3 \end{pmatrix}$, it is non-zero only when $m_1 + m_2 + m_3 = 0$ and when s_1, s_2, s_3 together satisfy the triangle inequality, $|s_1 - s_2| \leq s_3 \leq s_1 + s_2$. As such, the sum over m collapses, and $m = m_1 - m_3 = m_4 - m_2$.

However, this result is not shown in the literature. A more popular form is to express this formula in a *pair pseudopotentials*, which is widely used in the community of quantum Hall effect.

D. Haldane's pseudopotential

The pair pseudopotential $V^n(l)$ is defined as the interaction energy of a pair of electrons as a function of their pair angular momentum l. Although the pseudopotential is a function only of the pair angular momentum, $V^n(l)$ actually contains all of the correlative behaviors of any many-body system, and can be used in the place of the two-body matrix elements calculated above to perform the same calculations. The pseudopotential is defined on the

Haldane sphere by using standard angular momentum coupling to expand the monopole harmonics into a coupled basis,

$$|s, m_1; s, m_2\rangle = \sum_l |s, s; l, m_1 + m_2\rangle\langle s, s; l, m_1 + m_2|s, m_1; s, m_2\rangle$$

This is actually a momentum coupling transformation, and the coefficient $\langle s, s; l, m_1 + m_2|s, m_1; s, m_2\rangle$ is the ordinary Clebsch-Gordan coefficient.

If we expand both the initial and final state vectors in the coupled angular momentum basis, we can rewrite the two-body matrix element in the following form:

$$\begin{aligned}\langle s, m_1; s, m_2|V(r)|s, m_3; s, m_4\rangle \;=\; & \sum_{l,l'}\langle s, m_1; s, m_2|s, s; l, m_1 + m_2\rangle\langle s, s; l', m_3 + m_4|s, m_3; s, m_4\rangle \times \\ & \langle s, s; l, m_1 + m_2|V(\mathbf{r}_1 - \mathbf{r}_2)|s, s; l', m_3 + m_4\rangle\end{aligned}$$

In this expression, the pseudopotential for particles in a single Landau level is evaluated from the matrix element from

$$\langle s, s; l, m|V(r_1 - r_2)|s, s; l', m'\rangle\delta_{m=m_1+m_2}\delta_{m'=m_3+m_4}$$

For particles in the n th Landau level, that is, when $s = s_0 + n$ matrix element gives the pair pseudopotential.

In order to reduce the following expression slightly, we need lots of integral relations and results. We omit these tedious process, and reach the finial result:

$$\langle s, s; l, m|V(|r_1 - r_2|)|s, s; l', m'\rangle = V_s^{n=0}(l)\delta_{l,l'} = \delta_{l,l'}\sum_{k=0}^{2s} U_k(-)^{2s_0+l}(2s+1)^2 \begin{Bmatrix} l & s & s \\ k & s & s \end{Bmatrix} \begin{pmatrix} s & k & s \\ -s_0 & 0 & s_0 \end{pmatrix}^2 \tag{88}$$

where $s = s_0 + n$ is the shell angular momentum of the n-th Laudan level, l is the relative angular momentum between two particles. Here, $\begin{pmatrix} s & k & s \\ -s_0 & 0 & s_0 \end{pmatrix}$ is Wigner 3j coefficient and $\begin{Bmatrix} l & s & s \\ k & s & s \end{Bmatrix}$ is Wigner 6j coefficient. Please note that the expression of $V_s^n(l)$ does not depend on the relative angular momentum m, m'.

To sum up, the hamiltonian written by pseudopotential will be

$$H = \frac{1}{2} \sum_{m_1,m_2,m_3,m_4=-s}^{s} a^\dagger_{m_1,n} a^\dagger_{m_2,n} a_{m_3,n} a_{m_4,n} \delta_{m_1+m_2,m_3+m_4} \langle s, m_1; s, m_2|V|s, m_3; s, m_4\rangle$$

$$\langle s, m_1; s, m_2|V|s, m_3; s, m_4\rangle =$$

$$\sum_{l,l'} \langle s, m_1; s, m_2|s, s; l, m_1+m_2\rangle \langle s, s; l', m_3+m_4|s, m_3; s, m_4\rangle \times \langle s, s; l, m_1+m_2|V(\mathbf{r}_1-\mathbf{r}_2)|s, s; l', m_3+m_4$$

$$= \sum_l V_l \sqrt{2l+1}(-1)^{m_1+m_2} \begin{pmatrix} s & s & l \\ m_1 & m_2 & -m_1-m_2 \end{pmatrix} \sqrt{2l+1}(-1)^{m_3+m_4} \begin{pmatrix} s & s & l \\ m_3 & m_4 & -m_3-m_4 \end{pmatrix}$$

$$= \sum_l V_l (2l+1) \begin{pmatrix} s & s & l \\ m_1 & m_2 & -m_1-m_2 \end{pmatrix} \begin{pmatrix} s & s & l \\ m_3 & m_4 & -m_3-m_4 \end{pmatrix} \tag{89}$$

Let us calculate the pseudopotential using Eq. 88.

- For short-ranged interaction $V(r) = \delta(\mathbf{r})$, $U_k = 2k+1$, $V_s(l) = \begin{cases} \frac{(2s+1)^2}{(4s+1)}, l = 2s \\ 0, l \neq 2s \end{cases}$

- For short-ranged interaction $V(r) = \nabla^2\delta(\mathbf{r})$, $U_k = -k(k+1)(2k+1)$,

$$V_s(l) = \begin{cases} x_0 = -\frac{(1+s)^2(2s+1)^4((2s)!)^4}{s(4s+1)((2(s+1))!)^2((2s-1)!)^2} = -\frac{s(2s+1)^2}{4s+1} < 0, l = 2s \\ x_1 = \frac{4s(1+s)^2(2s+1)^4((2s)!)^2}{(4s-1)((2(s+1))!)^2} = \frac{s(2s+1)^2}{4s-1} > 0, l = 2s-1, \ \ [\lim_{s\to\infty} x_1 = s^2 + \frac{5}{4}s + \frac{9}{16}] \\ 0, others \end{cases} \tag{90}$$

- For coulomb interaction $V(r) = 1/r$, $U_k = 1$, $V^n_s(l) = \frac{2^{-2-4s}(2s+1)(2s+1)!((8s-1)/2)!}{((4s-1)/2)!(((4s+1)/2)!)^2}$

For coulomb interaction $V(r) = 1/r$, the above equation has a analytical form, first derived by Fano, for the lowest Landau level, $n = 0$:

$$V^{n=0}_s(l) = \frac{\begin{pmatrix} 4s_0 - 2l \\ 2s_0 - l \end{pmatrix} \begin{pmatrix} 4s_0 + 2l + 2 \\ 2s_0 + l + 1 \end{pmatrix}}{\begin{pmatrix} 4s_0 + 2 \\ 2s_0 + 1 \end{pmatrix}^2} \tag{91}$$

, which is widely used for calculation in first Laudau level.

E. Density operator

In the case of lowest Landau level ($s = s_0, n = 0$), we define the annihilation operator $\hat{\psi}(\theta, \varphi)$ on the projected Landau level as

$$\hat{\psi}(\theta, \varphi) = \sum_{m=-s}^{s} \overline{Y}_{s,m}^{(s_0)} \hat{c}_m. \tag{92}$$

$\hat{c}_m$ stands for the annihilation operator of Landau orbital m, and it is independent of coordinates (θ, φ). Monopole harmonics $Y_{l,m}^{(s_0)}$ see Eq. 72.

The density operator $\hat{n}(\theta, \varphi) = \hat{\psi}^\dagger \hat{\psi}$ can be written as,

$$\hat{n}(\theta, \varphi) = \sum_{m_1, m_2} Y_{s,m_1}^{(s_0)} \overline{Y}_{s,m_2}^{(s_0)} c_{m_1}^\dagger c_{m_2}. \tag{93}$$

Next we write the Hamiltonian in terms of density operator $n_{l,m}$ in the angular momentum space, defined as,

$$n(\theta, \varphi) = \sum_{m_1, m_2 = -s}^{s} \overline{Y}_{s,m_2}^{s_0} Y_{s,m_1}^{s_0} c_{m_1}^\dagger c_{m_2} = \sum_{l,m} n_{l,m} Y_{l,m}(\theta, \varphi). \tag{94}$$

Here $Y_{l,m}(\theta, \varphi) = Y_{l,m}^{(0)}$ is the spherical harmonics, with $m = -l, -l+1, \cdots, l$ and $l \in \mathbf{Z}$. $n_{l,m}$ can be obtained using spherical harmonic transformation,

$$\begin{aligned} n_{l,m} &= \int d\Omega\, \bar{Y}_{l,m}(\theta, \varphi) n(\theta, \varphi) \\ &= (2s+1)\sqrt{\frac{2l+1}{4\pi}} \sum_{m_1=-s}^{s} (-1)^{3s+m_1+l} \begin{pmatrix} s & l & s \\ m-m_1 & -m & m_1 \end{pmatrix} \begin{pmatrix} s & l & s \\ -s & 0 & s \end{pmatrix} c_{m_1}^\dagger c_{m_1-m} \\ &\overset{!}{=} (2s+1)\sqrt{\frac{2l+1}{4\pi}} \sum_{m_1=-s}^{s} (-1)^{3s+m_1+l} (-1)^{4s+2l} \begin{pmatrix} s & l & s \\ -m_1 & m & m_1-m \end{pmatrix} \begin{pmatrix} s & l & s \\ -s & 0 & s \end{pmatrix} c_{m_1}^\dagger c_{m_1-m}, \end{aligned} \tag{95}$$

where we used the integral in Eq. 86. Here $\begin{pmatrix} j_1 & j_2 & j_3 \\ m_1 & m_2 & m_3 \end{pmatrix}$ is the Wigner 3j-Symbol. To have the term $\begin{pmatrix} s & l & s \\ -m_1 & m & m_1-m \end{pmatrix}$ non-vanishing, we should have $l \leq 2s$. One can show that,

$$n_{l,m}^\dagger = (-1)^m n_{l,-m} \tag{96}$$

Relation between V_l and $\tilde{U}_l = U_l/(2l+1)$.—

For $\delta(\mathbf{r})$ potential

$$\begin{aligned} g_0\delta(\mathbf{r}) &\to U_l = g_0(2l+1), \tilde{U}_l = g_0 \\ g_0\delta(\mathbf{r}) &\to V_0 = g_0\frac{(2s+1)^2}{4s+1} \end{aligned} \tag{97}$$

and $\nabla^2\delta(\mathbf{r})$ potential

$$\begin{aligned} g_1\nabla^2\delta(\mathbf{r}) &\to U_l = g_1[-l(l+1)(2l+1)], \tilde{U}_l = g_1[-l(l+1)] \\ g_1\nabla^2\delta(\mathbf{r}) &\to V_0 = -g_1\frac{s(2s+1)^2}{4s+1}, V_1 = g_1\frac{s(2s+1)^2}{4s-1} \end{aligned} \tag{98}$$

For a pontential $g_0\delta(\mathbf{r}) + g_1\nabla^2\delta(\mathbf{r})$, we have the pseudopotential $\{V_0, V_1\}$ connected with $\{g_0, g_1\}$ as

$$\begin{cases} V_1 &= g_1\frac{s(2s+1)^2}{4s-1} \\ V_0 &= -g_1\frac{s(2s+1)^2}{4s+1} + g_0\frac{(2s+1)^2}{4s+1} \end{cases} \Rightarrow \begin{cases} g_0 &= \frac{4s+1}{(2s+1)^2}V_0 + \frac{4s-1}{(2s+1)^2}V_1 \\ g_1 &= \frac{4s-1}{s(2s+1)^2}V_1 \end{cases} \tag{99}$$

So in the language of $\tilde{U}_l$:

$$\Rightarrow \tilde{U}_l = g_0 - g_1 l(l+1) = \frac{4s+1}{(2s+1)^2}V_0 + \frac{4s-1}{(2s+1)^2}V_1 - \frac{4s-1}{s(2s+1)^2}V_1 \times l(l+1) \tag{100}$$

where $\tilde{U}_l$ is the parameter which pun in Eq. **??**.

Relation between two different expressions Eq. 89 and Eq. 87

$$\begin{aligned} &\langle s, m_1; s, m_2|V(r)|s, m_3; s, m_4\rangle = \\ &\sum_{l,l'}\langle s, m_1; s, m_2|s, s; l, m_1+m_2\rangle\langle s, s; l', m_3+m_4|s, m_3; s, m_4\rangle\times \\ &\langle s, s; l, m_1+m_2|V(\mathbf{r}_1-\mathbf{r}_2)|s, s; l', m_3+m_4\rangle \\ &= \sum_l V_l\sqrt{2l+1}(-1)^{-m_1-m_2}\begin{pmatrix} s & s & l \\ m_1 & m_2 & -m_1-m_2 \end{pmatrix}\sqrt{2l+1}(-1)^{-m_3-m_4}\begin{pmatrix} s & s & l \\ m_3 & m_4 & -m_3-m_4 \end{pmatrix} \\ &= \sum_l V_l(2l+1)\begin{pmatrix} s & s & l \\ m_1 & m_2 & -m_1-m_2 \end{pmatrix}\begin{pmatrix} s & s & l \\ m_3 & m_4 & -m_3-m_4 \end{pmatrix} \end{aligned} \tag{101}$$

$$\langle s,m_1;s,m_2|V|s,m_3;s,m_4\rangle = (2s+1)^2\sum_{k=0}^{k_{max}} U_k(-)^{2s+m_2+m_4}\times$$
$$\begin{pmatrix} s & k & s \\ -m_1 & m_1-m_4 & m_4 \end{pmatrix}\begin{pmatrix} s & k & s \\ -m_2 & m_2-m_3 & m_3 \end{pmatrix}\begin{pmatrix} s & k & s \\ -s & 0 & s \end{pmatrix}\begin{pmatrix} s & k & s \\ -s & 0 & s \end{pmatrix} \tag{102}$$

Next we apply the condition of (if j_1, j_2, j_3 satisfy the triangle condition)

$$(2j_3+1)\sum_{m_1,m_2}\begin{pmatrix} j_1 & j_2 & j_3 \\ m_1 & m_2 & m_3 \end{pmatrix}\begin{pmatrix} j_1 & j_2 & j_3' \\ m_1 & m_2 & m_3' \end{pmatrix} = \delta_{j3,j3'}\delta_{m_3,m_3'} \tag{103}$$

to the above to Equations, and get

$$\sum_l V_l\frac{1}{2l+1}\delta_{l,l'}\delta_{l,l''}\delta_{m'=-m_1-m_2}\delta_{m''=-m_3-m_4} = \sum_{k=0}^{k_{max}} U_k(2s+1)^2\begin{pmatrix} s & k & s \\ -s & 0 & s \end{pmatrix}^2\times$$
$$\sum_{m_1,m_2,m_3,m_4}(-)^{2s+m_2+m_4}\begin{pmatrix} s & k & s \\ -m_1 & m_1-m_4 & m_4 \end{pmatrix}\begin{pmatrix} s & k & s \\ -m_2 & m_2-m_3 & m_3 \end{pmatrix}$$
$$\begin{pmatrix} s & s & l \\ m_1 & m_2 & -m_1-m_2 \end{pmatrix}\begin{pmatrix} s & s & l \\ m_3 & m_4 & -m_3-m_4 \end{pmatrix}$$
$$\sum_{m_1,m_2,m_3,m_4}(-)^{2s+m_2+m_4}\begin{pmatrix} s & k & s \\ -m_1 & m_1-m_4 & m_4 \end{pmatrix}\begin{pmatrix} s & k & s \\ -m_2 & m_2-m_3 & m_3 \end{pmatrix}$$
$$\begin{pmatrix} s & s & l \\ m_1 & m_2 & -m_1-m_2 \end{pmatrix}\begin{pmatrix} s & s & l \\ m_3 & m_4 & -m_3-m_4 \end{pmatrix} \tag{104}$$

$$V_l \frac{1}{2l+1} = \sum_{k=0}^{k_{max}} U_k (2s+1)^2 (-)^{2s} \begin{pmatrix} s & k & s \\ -s & 0 & s \end{pmatrix}^2 \times \sum_{m_1,m_2,m_3,m_4} (-)^{m_2+m_4}$$
$$\begin{pmatrix} l & s & s \\ -m_1-m_2 & m_1 & m_2 \end{pmatrix} (-1)^{2s+l} \begin{pmatrix} l & s & s \\ m_3+m_4 & -m_3 & -m_4 \end{pmatrix}$$
$$(-1)^{2s+k} \begin{pmatrix} k & s & s \\ m_1-m_4 & -m_1 & m_4 \end{pmatrix} \begin{pmatrix} k & s & s \\ m_2-m_3 & m_3 & -m_2 \end{pmatrix}$$
$$= \sum_{k=0}^{k_{max}} U_k (2s+1)^2 (-)^{2s+l+k} \begin{pmatrix} s & k & s \\ -s & 0 & s \end{pmatrix}^2 \begin{Bmatrix} l & s & s \\ k & s & s \end{Bmatrix} \tag{105}$$

Here use the formula:

$$\begin{Bmatrix} j_1 & j_2 & j_3 \\ j_4 & j_5 & j_6 \end{Bmatrix} = \sum_{x_{i=1,..,6}} (-1)^{\sum_{k=1}^6 j_k - \sum_{k=1}^6 x_k} \begin{pmatrix} j_1 & j_2 & j_3 \\ -x_1 & -x_2 & -x_3 \end{pmatrix} \begin{pmatrix} j_1 & j_5 & j_6 \\ x_1 & -x_5 & x_6 \end{pmatrix} \times$$
$$\begin{pmatrix} j_4 & j_2 & j_6 \\ x_4 & x_2 & -x_6 \end{pmatrix} \begin{pmatrix} j_4 & j_5 & j_3 \\ -x_4 & x_5 & x_3 \end{pmatrix} \tag{106}$$

by setting $j_1 = l, j_4 = k, j_2 = j_3 = j_5 = j_6 = s$ and $x_1 = -m_1 - m_2 = -m_3 - m_4, x_2 =$

$m_3, x_3 = m_4, x_4 = m_2 - m_3 = -m_1 + m_4, x_5 = -m_1, x_6 = m_2$, to do the summation

$$\begin{aligned}
&\sum_{m_{1-4}} (-)^{m_2+m_4} \begin{pmatrix} l & s & s \\ -m_1-m_2 & m_1 & m_2 \end{pmatrix} \begin{pmatrix} l & s & s \\ m_3+m_4 & -m_3 & -m_4 \end{pmatrix} \\
&\begin{pmatrix} k & s & s \\ m_1-m_4 & -m_1 & m_4 \end{pmatrix} \begin{pmatrix} k & s & s \\ m_2-m_3 & m_3 & -m_2 \end{pmatrix} \\
&= \sum_{m_{1-6}} (-)^{m_2+m_4} \begin{pmatrix} l & s & s \\ m_5 & m_1 & m_2 \end{pmatrix} \begin{pmatrix} l & s & s \\ m_6 & -m_3 & -m_4 \end{pmatrix} \\
&\begin{pmatrix} k & s & s \\ m_1-m_4 & -m_1 & m_4 \end{pmatrix} \begin{pmatrix} k & s & s \\ m_2-m_3 & m_3 & -m_2 \end{pmatrix} \\
&= \sum_{m_{1-6}} (-)^{2m_2+2m_4-2m_1} (-)^{-(m_4+m_2-2m_1)} \begin{pmatrix} l & s & s \\ m_5 & m_1 & m_2 \end{pmatrix} \begin{pmatrix} l & s & s \\ m_6 & -m_3 & -m_4 \end{pmatrix} \\
&\begin{pmatrix} k & s & s \\ m_1-m_4 & -m_1 & m_4 \end{pmatrix} \begin{pmatrix} k & s & s \\ m_2-m_3 & m_3 & -m_2 \end{pmatrix} \\
&\overset{!}{=} \begin{Bmatrix} l & s & s \\ k & s & s \end{Bmatrix}
\end{aligned} \tag{107}$$

Similarly, we have

$$U_k = \frac{(-1)^{2s_0+k}(2k+1)^2}{(2s+1)^2} \begin{pmatrix} s & k & s \\ -s & 0 & s \end{pmatrix}^{-2} \sum_{l'=0}^{2s} \left[V_s(l')(-1)^{-l'}(2l'+1) \begin{Bmatrix} s & s & k \\ s & s & l' \end{Bmatrix} \right] \tag{108}$$

III. 2+1D TRANSVERSE ISING MODEL ON THE FUZZY SPHERE

Here we explicitly define the model, which is spinful electrons in the LLL. [40] In spatial space, the Hamiltonian takes the form

$$H = R^4 \int d\Omega_a d\Omega_b \, U(\Omega_{ab}) \left[n^0(\theta_a, \varphi_a) n^0(\theta_b, \varphi_b) - n^z(\theta_a, \varphi_a) n^z(\theta_b, \varphi_b) \right] - hR^2 \int d\Omega \, n^x(\theta, \varphi), \tag{109}$$

where $n^\alpha(\theta, \varphi)$ is a local density operator given by

$$n^\alpha(\theta, \varphi) = (\hat{\psi}^\dagger_\uparrow(\theta, \varphi), \, \hat{\psi}^\dagger_\downarrow(\theta, \varphi)) \, \sigma^\alpha \begin{pmatrix} \hat{\psi}_\uparrow(\theta, \varphi) \\ \hat{\psi}_\downarrow(\theta, \varphi), \end{pmatrix}, \tag{110}$$

with $\sigma^{x,y,z}$ being Pauli matrices, $\sigma^0 = I_{2\times 2}$, and $U(\Omega_{ab})$ the local density-density interactions (defined below). The first term behaves like an Ising ferromagnetic interaction, while the second term is the transverse field. By projecting the Hamiltonian into the LLL, we obtain

$$\begin{aligned} H &= H_{00} + H_{zz} + H_t, \\ H_{00} &= \frac{1}{2} \sum_{m_{1,2,3,4}=-s}^{s} V_{m_1,m_2,m_3,m_4} \left(\mathbf{c}^\dagger_{m_1} \mathbf{c}_{m_4} \right) \left(\mathbf{c}^\dagger_{m_2} \mathbf{c}_{m_3} \right) \delta_{m_1+m_2,m_3+m_4}, \\ H_{zz} &= -\frac{1}{2} \sum_{m_{1,2,3,4}=-s}^{s} V_{m_1,m_2,m_3,m_4} \left(\mathbf{c}^\dagger_{m_1} \sigma^z \mathbf{c}_{m_4} \right) \left(\mathbf{c}^\dagger_{m_2} \sigma^z \mathbf{c}_{m_3} \right) \delta_{m_1+m_2,m_3+m_4}, \\ H_t &= -h \sum_{m=-s}^{s} \mathbf{c}^\dagger_m \sigma^x \mathbf{c}_m, \end{aligned} \tag{111}$$

where $\mathbf{c}^\dagger_m = (c^\dagger_{m\uparrow}, c^\dagger_{m\downarrow})$ is the fermion creation operator on the m_{th} Landau orbital. The parameter V_{m_1,m_2,m_3,m_4} is connected to the Haldane pseudopotential V_l by

$$V_{m_1,m_2,m_3,m_4} = \sum_l V_l \, (4s - 2l + 1) \begin{pmatrix} s & s & 2s-l \\ m_1 & m_2 & -m_1-m_2 \end{pmatrix} \begin{pmatrix} s & s & 2s-l \\ m_4 & m_3 & -m_3-m_4 \end{pmatrix}, \tag{112}$$

where $\begin{pmatrix} j_1 & j_2 & j_3 \\ m_1 & m_2 & m_3 \end{pmatrix}$ is the Wigner $3j$-symbol. In this paper we will only consider ultra-local density-density interactions in real space, i.e. $U(\Omega_{ab}) = g_0 \frac{1}{R^2} \delta(\Omega_{ab}) + g_1 \frac{1}{R^4} \nabla^2 \delta(\Omega_{ab})$, and the associated Haldane pseudopotentials involve V_0, V_1. Next we will set $V_1 = 1$ as energy unit and vary V_0, h to study the phase diagram.

We consider the half-filling case with the LLL filled by $N = 2s + 1$ electrons. When $h = 0$ and $V_0, V_1 > 0$, the ground state is an Ising ferromagnet that spontaneously breaks

$\mathbf{Z}_2$ symmetry. In quantum Hall literature this phase is called quantum Hall ferromagnetism [41, 42]. The two-fold degenerate ground states are $|\Psi_\uparrow\rangle = \prod_{m=-s}^{s} c_{m\uparrow}^\dagger|0\rangle$ and $|\Psi_\downarrow\rangle = \prod_{m=-s}^{s} c_{m\downarrow}^\dagger|0\rangle$. When $h \gg V_0, V_1$, the ground state is a trivial paramagnet that preserves Ising symmetry, $|\Psi_x\rangle = \prod_{m=-s}^{s}(c_{m\uparrow}^\dagger + c_{m\downarrow}^\dagger)|0\rangle$. Therefore, we expect a $2+1D$ Ising transition as increasing h. The global phase diagram of the model is as shown in Fig. 6(b).

Space-time symmetry of Ising.

1. Particle-hole symmetry: $\mathbf{c}_m \to i\sigma^y \mathbf{c}_m^\dagger$, $i \to -i$. That is: $c_{m,\uparrow} \to c_{m,\downarrow}^\dagger, c_{m,\downarrow} \to -c_{m,\uparrow}^\dagger$, $c_{m,\uparrow}^\dagger \to c_{m,\downarrow}, c_{m,\downarrow}^\dagger \to -c_{m,\uparrow}$.

The particle-hole symmetry turns out to be the spacetime parity symmetry of 3D Ising CFT. To understand this relation, we can write an $SO(3)$ vector,

$$n_{m=0,\pm1}^x = \sum_{m_1=-s}^{s} (-1)^{m_1} \begin{pmatrix} s & s & 1 \\ m_1 & m-m_1 & -m \end{pmatrix} \mathbf{c}_{m_1}^\dagger \sigma^x \mathbf{c}_{m_1-m}, \tag{113}$$

and find it transforms as

$$n_{m=0}^x = \sum_{m_1=-s}^{s} (-1)^{m_1} \begin{pmatrix} s & s & 1 \\ m_1 & -m_1 & 0 \end{pmatrix} (c_{m_1\uparrow}^\dagger c_{m_1\downarrow} + c_{m_1\downarrow}^\dagger c_{m_1\uparrow}) \tag{114}$$

$$\to \sum_{m_1=-s}^{s} (-1)^{m_1} \begin{pmatrix} s & s & 1 \\ m_1 & -m_1 & 0 \end{pmatrix} (-c_{m_1\downarrow} c_{m_1\uparrow}^\dagger - c_{m_1\uparrow} c_{m_1\downarrow}^\dagger) = n_{m=0}^x \tag{115}$$

and

$$n_{m=1}^x = \sum_{m_1=-s}^{s} (-1)^{m_1} \begin{pmatrix} s & s & 1 \\ m_1 & 1-m_1 & -1 \end{pmatrix} (c_{m_1\uparrow}^\dagger c_{m_1-1\downarrow} + c_{m_1\downarrow}^\dagger c_{m_1-1\uparrow}) \tag{116}$$

$$\to \sum_{m_1=-s}^{s} (-1)^{m_1} \begin{pmatrix} s & s & 1 \\ m_1 & 1-m_1 & -1 \end{pmatrix} (-c_{m_1\downarrow} c_{m_1-1\uparrow}^\dagger - c_{m_1\uparrow} c_{m_1-1\downarrow}^\dagger) \tag{117}$$

$$= \sum_{m_1=-s}^{s} (-1)^{m_1} \begin{pmatrix} s & s & 1 \\ m_1 & 1-m_1 & -1 \end{pmatrix} (c_{m_1-1\uparrow}^\dagger c_{m_1\downarrow} + c_{m_1-1\downarrow}^\dagger c_{m_1\uparrow}) \tag{118}$$

$$= \sum_{m_1=-s}^{s} (-1)^{m_1+1} \begin{pmatrix} s & s & 1 \\ m_1+1 & -m_1 & -1 \end{pmatrix} (c_{m_1\uparrow}^\dagger c_{m_1+1\downarrow} + c_{m_1\downarrow}^\dagger c_{m_1+1\uparrow}) \tag{119}$$

$$= -\sum_{m_1=-s}^{s} (-1)^{m_1} \begin{pmatrix} s & s & 1 \\ m_1 & -1-m_1 & 1 \end{pmatrix} (c_{m_1\uparrow}^\dagger c_{m_1+1\downarrow} + c_{m_1\downarrow}^\dagger c_{m_1+1\uparrow}) = -n_{m=-1} \tag{120}$$

$$\begin{pmatrix} n^x_{m=1} \\ n^x_{m=0} \\ n^x_{m=-1} \end{pmatrix} \to \begin{pmatrix} 0 & 0 & -1 \\ 0 & 1 & 0 \\ -1 & 0 & 0 \end{pmatrix} \begin{pmatrix} n^x_{m=1} \\ n^x_{m=0} \\ n^x_{m=-1} \end{pmatrix}, \tag{121}$$

under particle-hole transformation. Since $\det[\begin{pmatrix} 0 & 0 & -1 \\ 0 & 1 & 0 \\ -1 & 0 & 0 \end{pmatrix}] = -1$, The particle-hole acts as an improper Z_2 of $O(3)$, so it can be identified as the spacetime parity of the 3D Ising CFT.

A. Symmetries

The Hamiltonian (111) has three symmetries,

1. Ising $\mathbf{Z}_2$ symmetry: $\mathbf{c}_m \to \sigma^x \mathbf{c}_m$.

2. $SO(3)$ sphere rotation symmetry: $\mathbf{c}_{m=-s,\cdots,s}$ form the spin-s representation of $SO(3)$.

3. Particle-hole symmetry: $\mathbf{c}_m \to i\sigma^y \mathbf{c}^*_m$, $i \to -i$.

To further analyze the Ising transition in our system, we will relate the UV symmetries of our Landau level model to the IR symmetries of the 3D Ising CFT. It is obvious we can identify the Ising $\mathbf{Z}_2$ and $SO(3)$ sphere rotation between UV and IR. A slightly non-trivial symmetry is the particle-hole symmetry, which turns out to be the spacetime parity symmetry of 3D Ising CFT. To understand this relation, we can write an $SO(3)$ vector,

$$n^x_{m=0,\pm 1} = \sum_{m_1=-s}^{s} (-1)^{m_1} \begin{pmatrix} s & s & 1 \\ m_1 & m-m_1 & -m \end{pmatrix} \mathbf{c}^\dagger_{m_1} \sigma^x \mathbf{c}_{m_1-m}, \tag{122}$$

and find it transforms as

$$\begin{pmatrix} n^x_{m=1} \\ n^x_{m=0} \\ n^x_{m=-1} \end{pmatrix} \to \begin{pmatrix} 0 & 0 & -1 \\ 0 & 1 & 0 \\ -1 & 0 & 0 \end{pmatrix} \begin{pmatrix} n^x_{m=1} \\ n^x_{m=0} \\ n^x_{m=-1} \end{pmatrix}, \tag{123}$$

under particle-hole transformation. The particle-hole acts as an improper $\mathbf{Z}_2$ of $O(3)$, so it can be identified as the spacetime parity of the 3D Ising CFT.

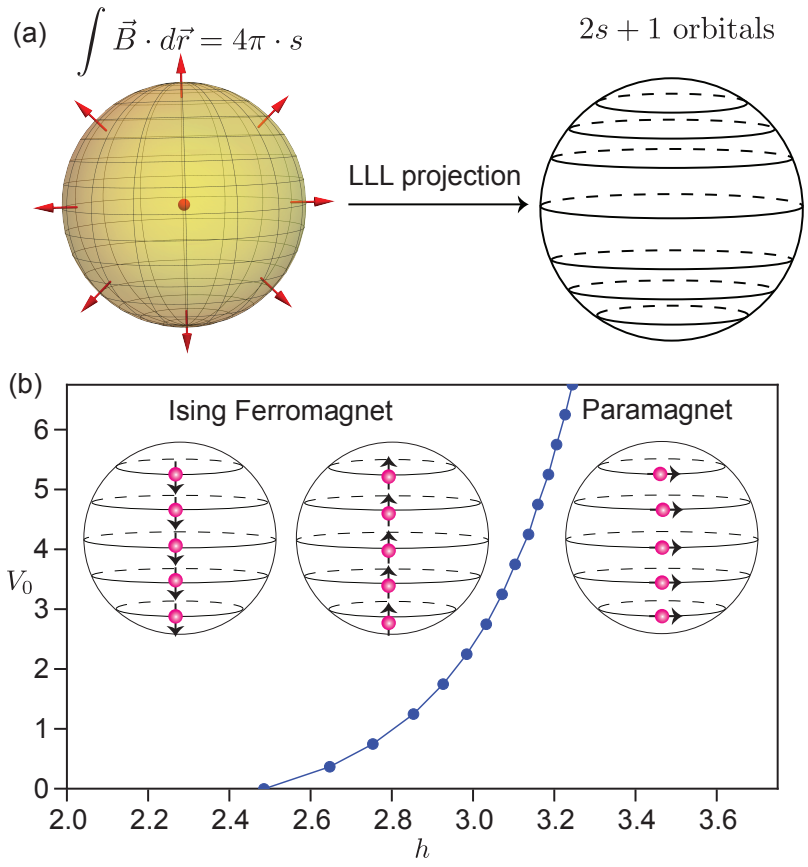

FIG. 6. (a) Schematic plot of electrons moving on a sphere in the presence of $4\pi \cdot s$ monopole. The LLL has $2s+1$ degenerate orbitals, which form an $SO(3)$ spin-s irreducible representation. A system projected into the LLL can be equivalently viewed as a fuzzy sphere. (b) Phase diagram of the proposed model consisting of a continuous phase transition from a quantum Hall Ising ferromagnet to a disordered paramagnet.

B. Order parameter

Electric charges of fermions are gapped in the entire phase diagram, while the Ising spins of fermions are the degrees of freedom that go through the phase transitions. Therefore, all the gapless degrees of freedom at the phase transition are charge-neutral. In particular, the order parameter of the transition is a particle-hole excitation of fermions,

$$M = \sum_{m=-s}^{s} \mathbf{c}_m^\dagger \frac{\sigma^z}{2} \mathbf{c}_m. \tag{124}$$

We emphasize an important point for the Landau level regularization of the Ising transition: the electrons are sitting on a fuzzy sphere due to the monopole, but the Ising spins are

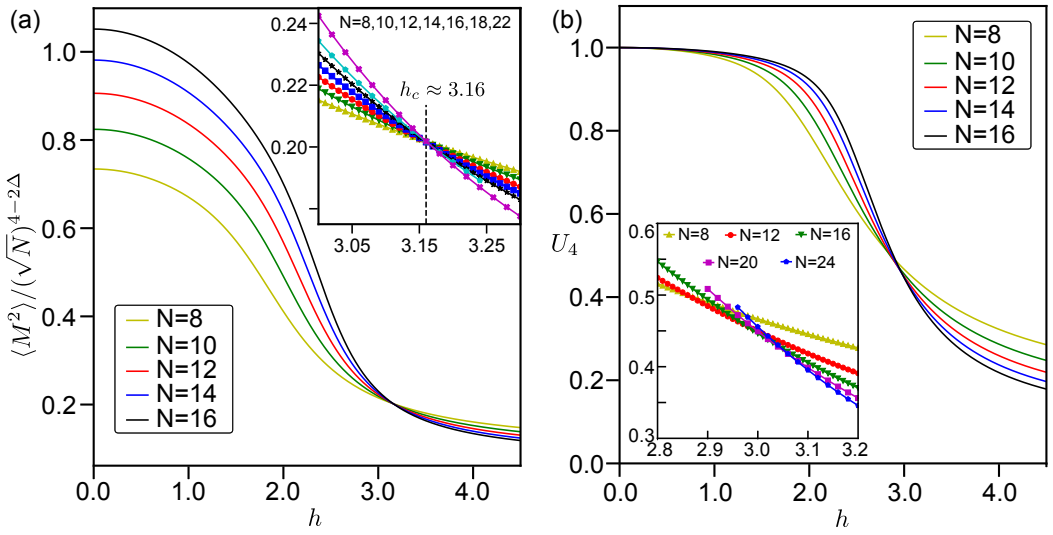

FIG. 7. (a) Finite size scaling of order parameter $\langle M^2\rangle/N^{2-\Delta}$. $\Delta = 0.518148$ is the scaling dimension of the Ising order parameter field. $N = 2s+1$ is the number of electrons (i.e. Ising spins), hence it should be identified as space volume and the length scale is $\sim \sqrt{N}$. The rescaled order parameter perfectly crosses at the same point $h_c \approx 3.16$. (b) Plot of the RG-invariant binder cumulant U_4. The binder cumulant does not stably cross at the same point due to the large finite size effect. We set $V_0 = 4.75$ here.

sitting on a normal sphere (for any finite $N = 2s+1$) since they are charge neutral. This is the key difference between our Landau level regularization and the non-commutative field theory [43], namely the latter always has quantum fields defined on a fuzzy manifold as long as the physical volume is finite.

C. Finite size scaling

The phase diagram in Fig. 6(b) is obtained by the conventional finite size scaling of the $\mathbf{Z}_2$ order parameter M in Eq. (124). We have simulated $N = 2s+1 = 8, 10, \cdots 24$ using ED for smaller sizes ($N \leq 16$) and DMRG for larger sizes $N > 16$ (the length scale in this $2+1$D system is $L_x = \sqrt{N}$). At the phase transition point, the $\mathbf{Z}_2$ order parameter should scale as $\langle M^2\rangle \sim L_x^{4-2\Delta} = N^{2-\Delta}$ [44], where $\Delta \approx 0.5181489$ is the scaling dimension of Ising order parameter [11, 45]. Fig. 7 (a) depicts $\langle M^2\rangle/N^{2-\Delta}$ with respect with the transverse field strength h of different N for $V_0 = 4.75$. All the curves nicely cross at $h_c \approx 3.16$, which we identify as the transition point. Similarly for other V_0 we have identified the critical h_c

and obtained the phase diagram as shown in Fig. 6(b).

We have also computed the binder cumulant

$$U_4 = \frac{3}{2}\left(1 - \frac{1}{3}\frac{\langle M^4\rangle}{\langle M^2\rangle^2}\right). \tag{125}$$

U_4 is a RG-invariant quantity, and $U_4 = 1, 0$ at the thermodynamic limit corresponds to the ordered phase and disordered phase, respectively. At the phase transition U_4 will be a universal quantity related to the four point correlator of the order parameter field σ of CFT [46]. Fig. 7 (b) shows U_4 with respect to the transverse field strength h for different N for $V_0 = 4.75$. Clearly, at small h the model is in the Ising ferromagnetic phase, while at large h the model is in the disordered phase. To estimate the value of binder ratio at the critical point U_4^c, we perform a detailed crossing-point analysis (Appendix Sec. **??**). With the data on hand, the best estimate we can give is $0.28 \leq U_4^c \leq 0.40$. It will be interesting to evaluate U_4 from conformal bootstrap and compare with our estimate.

In practice, for small N (as we simulated numerically), finite-size effects are inevitable. One common source is from the couplings of irrelevant operators, which are typically present in microscopic models. Tuning along the critical line in the 2-dimensional parameter space (V_0, h) shown in Fig. 6(b) generically modifies the coupling strength of irrelevant operators and therefore the magnitude of finite-size effects (while the relevant operators flow to the same fixed point). In the following section, we will present the data of the state-operator correspondence at a particular point $V_0 = 4.75, h_c = 3.16$, where we find the finite size effects are smallest.

D. Operator spectra

We now turn to the central results of our paper: the state-operator correspondence of the $3D$ Ising transition. As explained in previous Sec, on $S^2 \times R$ the eigenstates of the quantum Hamiltonian are in one-to-one correspondence with the scaling operators of its corresponding CFT. In particular, the energy gaps of each state will be proportional to the scaling dimensions of the scaling operators. Therefore, we explore energy spectra at the critical point by utilizing exact diagonalization and compare it with CFT predictions.

To match the Ising transition's energy spectra with the $3D$ Ising CFT's operator spectrum, we first need to rescale the energy spectrum with a non-universal (i.e. model- and

size-dependent) numerical factor. The natural calibrator is the energy momentum tensor $T_{\mu_1\mu_2}$, a conserved operator that any local CFT possesses. For any $3D$ CFT, $T_{\mu_1\mu_2}$ will be a global symmetry singlet, Lorentz spin $\ell = 2$ operator with scaling dimension $\Delta_T = 3$. Our model has exact $SO(3)$ Lorentz rotation, Ising Z_2, and spacetime parity symmetries, so every eigenstate has well-defined quantum numbers (Z_2, P, ℓ) of these three symmetries. The energy-momentum tensor will be the lowest state in the $(Z_2 = 1, P = 1, \ell = 2)$ sector. We rescale the full spectrum by setting the energy momentum tensor to exactly $\Delta_T = 3$, and then examine if the low-lying states form representations of $3D$ conformal symmetry up to a finite size correction.

To facilitate later analysis of our numerical results, we will elaborate a bit more about the operator contents of a $3D$ CFT. In $3D$ the Lorentz rotation group is the familiar $SO(3)$ group, all the irreducible representations of which are rank-ℓ symmetric traceless representations, i.e., spin-ℓ representations. So all (primary and descendant) operators have two quantum numbers (Δ, ℓ). A primary operator O with quantum number $\ell = 0$ is called a scalar operator, and any of its descendants can be written as

$$\partial_{\nu_1} \cdots \partial_{\nu_j} \Box^n O, \quad n, j \geq 0, \tag{126}$$

with quantum number $(\Delta + 2n + j, j)$. We note $\Box = \partial^2$. Here and hereafter all the free indices shall be symmetrized with the trace subtracted. The descendants of a spin-ℓ primary operator $O_{\mu_1 \cdots \mu_\ell}$ are a bit more complicated as there are two different types. The first type can be written as,

$$\partial_{\nu_1} \cdots \partial_{\nu_j} \partial_{\mu_1} \cdots \partial_{\mu_i} \Box^n O_{\mu_1 \cdots \mu_\ell}, \tag{127}$$

with quantum number $(\Delta + 2n + j + i, \ell + j - i)$ for $\ell \geq i \geq 0,\ n, j \geq 0$. Here and hereafter the repeated indices shall be contracted. The other type will involve the ε tensor of $SO(3)$, and can be written as,

$$\varepsilon_{\mu_l \rho \tau} \partial_\rho \partial_{\nu_1} \cdots \partial_{\nu_j} \partial_{\mu_1} \cdots \partial_{\mu_i} \Box^n O_{\mu_1 \cdots \mu_\ell}, \tag{128}$$

with quantum number $(\Delta + 2n + j + i + 1, \ell + j - i)$ for $\ell - 1 \geq i \geq 0,\ n, j \geq 0$. We note that the ε tensor alters spacetime parity symmetry of $O_{\mu_1 \cdots \mu_\ell}$.

We also remark that conserved operators (i.e. global symmetry current J_μ and energy momentum tensor $T_{\mu\nu}$) should be treated a bit differently, because they satisfy the conser-

TABLE I. Low-lying primary operators identified via state-operator correspondence on a fuzzy sphere with $N = 16$ electrons. The operators in the first and second row are Z_2 odd and even operators, respectively. We highlight that two new parity-odd primary operators σ^{P-} and ϵ^{P-} are found. The conformal bootstrap data is from Ref. [45].

	σ	σ'	$\sigma_{\mu_1\mu_2}$	$\sigma'_{\mu_1\mu_2}$	$\sigma_{\mu_1\mu_2\mu_3}$	$\sigma_{\mu_1\mu_2\mu_3\mu_4}$		σ^{P-}
Bootstrap	0.518	5.291	4.180	6.987	4.638	6.113		NA
Fuzzy sphere	0.524	5.303	4.214	7.048	4.609	6.069		11.191
	ϵ	ϵ'	ϵ''	$T_{\mu\nu}$	$T'_{\mu\nu}$	$\epsilon_{\mu_1\mu_2\mu_3\mu_4}$	$\epsilon'_{\mu_1\mu_2\mu_3\mu_4}$	ϵ^{P-}
Bootstrap	1.413	3.830	6.896	3	5.509	5.023	6.421	NA
Fuzzy sphere	1.414	3.838	6.908	3	5.583	5.103	6.347	10.014

vation equations $\partial_\mu J_\mu = 0$ and $\partial_\mu T_{\mu\nu} = 0$. Therefore, their descendants in Eq. (127) and (128) should have $i = 0$. [47]

We analyze the low-lying spectra according to the following steps,

1. For each $Z_2 = \pm 1$ sector, we find the lowest-lying energy state (regardless of ℓ and P), and identify it as a primary state.

2. Based on the representation theory of the 3D conformal group as summarized in Eq. (126), (127), (128), we enumerate the descendant states of the identified primary state and examine if all of descendant states (up to $\Delta = 7$) exist in our energy spectrum.

3. We remove the identified conformal multiplet (i.e. primary and its descendants) from the energy spectrum, and for the remaining states we repeat the step 1,2.

Remarkably, we found that the lowest-lying 70 eigenstates [48] form representations of the 3D conformal symmetry up to a small finite size correction, with no extra or missing state. This is a direct and unambiguous demonstration of the emergent conformal symmetry of the $3D$ Ising transition.

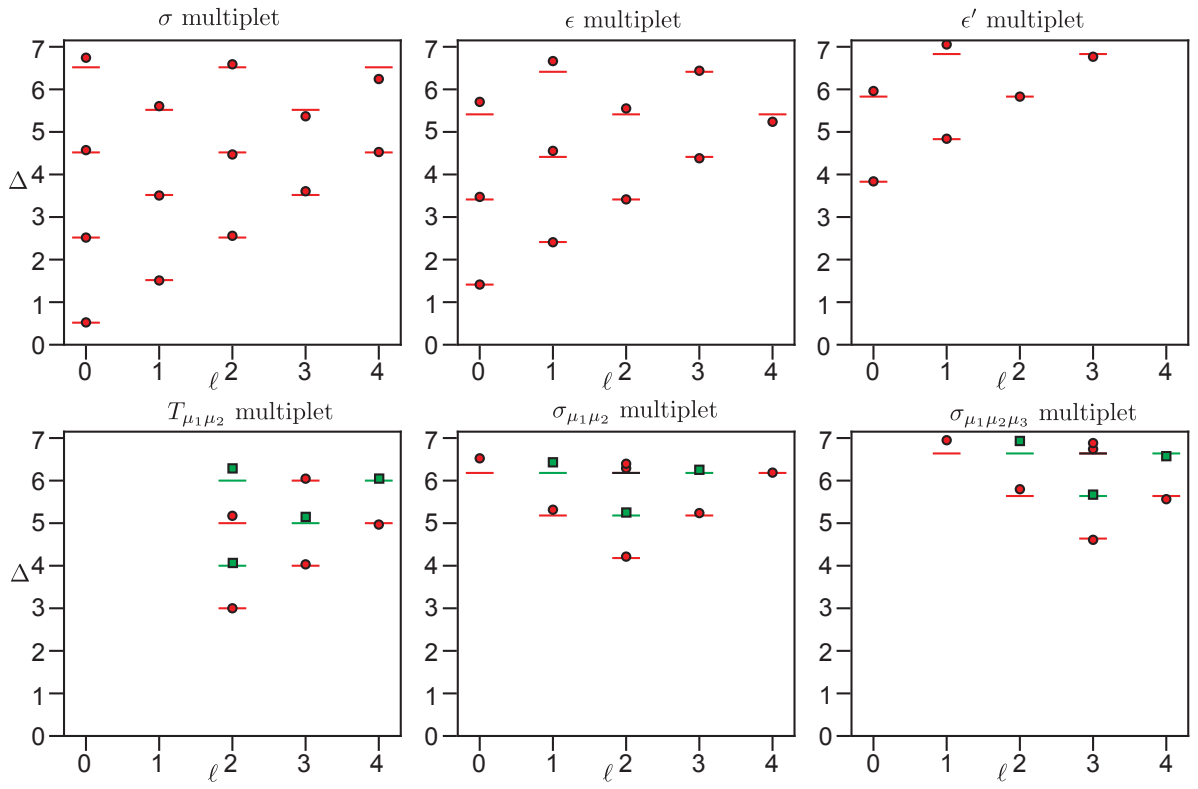

FIG. 8. Conformal multiplet of several low lying primary operators: scaling dimension Δ versus Lorentz spin ℓ. We plot conformal bootstrap data with lines: lines in red are parity even, non-degenerate operators; lines in green are parity odd, non-degenerate operators; lines in black are parity even, two-fold degenerate operators. Symbols are our numerical data of parity even (red circle) and odd (green square) operators. The discrepancy is typically more significant for the larger Δ.

After verifying the emergent conformal symmetry, we further compare our scaling dimensions of the identified primary operators with the numerical conformal bootstrap data [11, 45], and we find a good agreement for all of them. Table I lists all the primary operators we have identified with $N = 16$ ED data. We have found 12 parity-even primary operators besides the energy-momentum tensor, and all of them have less than a 1.6% discrepancy from the bootstrap data [11, 45]. As one can see the numerical accuracy is unexpectedly high, particularly given that it is from a small system size ($N = 16$ total spins): around 10 operators have relative numerical error around $3\% \sim 5.5\%$, and the rest of them have relative numerical error smaller than 3%. Fig. 8 plots conformal multiplets of a few representative primary operators, which clearly illustrate the emergent conformal symmetry and

agree well with numerical conformal bootstrap results.

A few remarks are in order. 1) We verify the emergent conformal symmetry of the $3D$ Ising transition by showing that the low-lying spectra of our model form representations of $3D$ conformal symmetry. This procedure does not rely on any input of previous knowledge such as numerical bootstrap data. 2) A spinning ($\ell > 0$) parity-even (parity-odd) primary operator can have parity-odd (parity-even) descendant opertors as written in Eq. (128). This nontrivial structure from the CFT's algebra matches our ED spectrum. [49] 3) The energy momentum tensor $T_{\mu_1\mu_2}$ is a conserved operator, so it does not have any $\ell < 2$ descendant. This structure is clearly shown in our data. 4) All the parity-even primary operators that we found have been reported in the bootstrap study of mixed correlators $\langle\sigma\sigma\sigma\sigma\rangle$, $\langle\epsilon\epsilon\epsilon\epsilon\rangle$, $\langle\sigma\sigma\epsilon\epsilon\rangle$. The mixed-correlator bootstrap study is only capable of detecting operators in the $\sigma \times \sigma$, $\epsilon \times \epsilon$ and $\sigma \times \epsilon$ OPE, so it will miss $(Z_2 = 1, P = 1, \text{odd}\, \ell)$ primary operators (in addition to $P = -1$ primaries). Our approach should be able to detect operators in these quantum number sectors, including the candidate of virial current [50] [51], namely the lowest primary in the $(\mathbb{Z}_2 = 1, P = 1, \ell = 1)$ sector. We have not observed any primary operators in the $(\mathbb{Z}_2 = 1, P = 1, \text{odd}\, \ell)$ sector below $\Delta = 7$, and so this gives a lower bound for the virial current candidate, which is higher than the previous estimate [52]. 5) We have identified two previously unknown (parity-odd) primary operators in the $(\mathbb{Z}_2 = 1, P = -1, \ell = 0)$ and $(\mathbb{Z}_2 = -1, P = -1, \ell = 0)$ sectors with $\Delta \approx 10.01$ and $\Delta \approx 11.19$, respectively. To access $P = -1$ primary operators in the bootstrap calculation, one has to bootstrap correlation functions of the spinning operator: for example, the energy momentum tensor. Such study has only been initiated in Ref. [53] but no $P = -1$ primary has been identified by conformal bootstrap or any other methods so far. 6) In all previous lattice model studies, only several primary fields (σ, ϵ and ϵ') were found, and their scaling dimensions are related to the critical exponents η, ν and ω [44, 54].

E. OPE coefficients

1. $\langle 0|\hat{\phi}|\phi\rangle$

First, we consider the scalar-scalar correlation function on $\mathbb{R}^d$,

$$\langle 0|\hat{\phi}(r,\Omega)\hat{\phi}(r',\Omega')|0\rangle = \frac{1}{(r^2 + r'^2 - 2rr'\cos(\Omega - \Omega'))^{\Delta}}, \tag{129}$$

where (r, Ω) are the spherical coordinates and Δ is the scaling dimension of field $\hat{\phi}$. Using the relation of state-operate correspondence

$$|\phi\rangle = \lim_{r\to 0} \hat{\phi}(r,\Omega)|0\rangle, \qquad \langle\phi| = \lim_{r\to\infty} r^{2\Delta}\langle 0|\hat{\phi}(r,\Omega), \tag{130}$$

we have

$$\langle 0|\hat{\phi}(r,\Omega)|\phi\rangle = \lim_{r'\to 0}\langle 0|\hat{\phi}(r,\Omega)\hat{\phi}(r',\Omega')|0\rangle = \frac{1}{r^{2\Delta}}. \tag{131}$$

Then, we apply the Weyl-transformation $\tau = R\ln r$ to map (r,Ω) in $\mathbb{R}^d$ to (τ,Ω) in $S^{d-1}\times\mathbb{R}$, where R is the radius of S^{d-1}. The operator transforms as

$$\hat{\phi}(r,\Omega) \to \hat{\phi}(\tau,\Omega) = \Lambda(r,\Omega)^{\Delta/2}\hat{\phi}(r,\Omega), \tag{132}$$

where $\Lambda = R^{-2}e^{\frac{2\tau}{R}}$ is the scale factor of this transformation and we can see it by considering the metric

$$ds^2 = dr^2 + r^2 d\Omega^2 = R^{-2}e^{\frac{2\tau}{R}}\left(d\tau^2 + R^2 d\Omega^2\right) = \Lambda(r,\Omega)\left(d\tau^2 + R^2 d\Omega^2\right). \tag{133}$$

Substituting into the correlator and letting $\tau = 0$, we finally get

$$\langle 0|\hat{\phi}(\tau=0,\Omega)|\phi\rangle = \langle 0|\Lambda(r,\Omega)^{\Delta/2}\hat{\phi}(r,\Omega)|\phi\rangle\big|_{r=1} = \Lambda(r,\Omega)^{\Delta/2}\frac{1}{r^{2\Delta}}\big|_{r=1} = R^{-\Delta}. \tag{134}$$

2. $\langle\phi_1|\hat{\phi}_2|\phi_3\rangle$

Now we consider the scalar-scalar-scalar correlator

$$\langle 0|\hat{\phi}_i(r_i,\Omega_i)\hat{\phi}_j(r_j,\Omega_j)\hat{\phi}_k(r_k,\Omega_k)|0\rangle = \frac{f_{ijk}}{d_{ij}^{\Delta_i+\Delta_j-\Delta_k}d_{jk}^{-\Delta_i+\Delta_j+\Delta_k}d_{ik}^{\Delta_i-\Delta_j+\Delta_k}}, \tag{135}$$

where $d_{12} = \sqrt{r_1^2 + r_2^2 - 2r_1r_2\cos(\Omega_1-\Omega_2)}$ is the distance between (r_1,Ω_1) and (r_2,Ω_2) . Using state-operator correspondence relations Eq. (130) we have

$$\langle\phi_i|\hat{\phi}_j(r_j,\Omega_j)|\phi_k\rangle = \lim_{r_i\to\infty, r_k\to 0} r_i^{2\Delta_i}\langle 0|\hat{\phi}_i(r_i,\Omega_i)\hat{\phi}_j(r_j,\Omega_j)\hat{\phi}_k(r_k,\Omega_k)|0\rangle = \frac{f_{ijk}}{r_j^{-\Delta_i+\Delta_j+\Delta_k}}. \tag{136}$$

Similarly, under the Weyl-transformation

$$\langle\phi_i|\hat{\phi}_j(\tau=0,\Omega)|\phi_k\rangle = f_{ijk}R^{-\Delta_j}. \tag{137}$$

Thus, one can compute the OPE coefficients through Eq. 134 and Eq. 137

$$f_{ijk} = \frac{\langle\phi_i|\hat{\phi}_j(\tau=0,\Omega)|\phi_k\rangle}{\langle 0|\hat{\phi}(\tau=0,\Omega)|\phi\rangle}. \tag{138}$$

3. OPE coefficients and finite-size scaling

In this section, we will present a detailed analysis of OPE coefficients from the microscopic spin operators. Generally speaking, since spin operators we used are not the exact CFT primary fields, so the three-point correlators involve contributions from other primaries or descendants. Fortunately, we will show that many OPE coefficients can be extracted from the proper finite-size extrapolation.

We will choose local operator $\hat{n}^z(\Omega)$ to approach the CFT operator $\hat{\sigma}$, and $\hat{n}^x(\Omega)$, $\hat{O}_\epsilon(\Omega)$ to approach $\hat{\epsilon}$. Although CFT operators and spin operators are always local operators defined on the sphere, for computing OPE coefficients it is more convenient to use operators defined in the angular momentum (orbital) space, which are the spherical modes of the local operators, e.g.,

$$\hat{O}_{l,m} = \int d\Omega\, \bar{Y}_{l,m}(\Omega)\hat{O}(\Omega). \tag{139}$$

So in the detailed analysis presented below, the computations are done in the orbital space.

1. $f_{\sigma\sigma\epsilon}$

The operator decomposition $n^z(\mathbf{\Omega})$ generically is,

$$\begin{aligned}\hat{n}^z(\mathbf{\Omega}) = {} & c_\sigma\hat{\sigma}(\mathbf{\Omega}) + c_{\partial_\mu\sigma}\partial_\mu\hat{\sigma}(\mathbf{\Omega}) + c_{\Box\sigma}\Box\hat{\sigma}(\mathbf{\Omega}) + c_{\partial_\mu\partial_\nu\sigma}\partial_\mu\partial_\nu\hat{\sigma}(\mathbf{\Omega}) + \cdots \\ & + c_{\sigma_{\mu\nu}}\hat{\sigma}_{\mu\nu}(\mathbf{\Omega}) + c_{\partial_\mu\sigma_{\mu\nu}}\partial_\mu\hat{\sigma}_{\mu\nu}(\mathbf{\Omega}) + c_{\partial_\rho\sigma_{\mu\nu}}\partial_\rho\hat{\sigma}_{\mu\nu}(\mathbf{\Omega}) + \cdots \\ & + c_{\sigma'}\hat{\sigma}'(\mathbf{\Omega}) + c_{\partial_\mu\sigma'}\partial_\mu\hat{\sigma}'(\mathbf{\Omega}) + c_{\Box\sigma'}\Box\hat{\sigma}'(\mathbf{\Omega}) + c_{\partial_\mu\partial_\nu\sigma'}\partial_\mu\partial_\nu\hat{\sigma}'(\mathbf{\Omega}) + \cdots \\ & + \cdots\end{aligned} \tag{140}$$

where each line represents components of a primary and its descendants, the conformal dimension of these operators are $\Delta_{\hat{\sigma}} \approx 0.51814$, $\Delta_{\hat{\sigma}'} \approx 5.2906$, and $\Delta_{\sigma_{\mu\nu}} \approx 4.1803$ and more other operators included in $\cdots$. Thus, the OPE coefficient can be extracted by $\frac{\langle\sigma|\hat{n}^z_{0,0}|\epsilon\rangle}{\langle\sigma|\hat{n}^z_{0,0}|0\rangle}$ for which only scalar scaling operators will contribute,

$$\begin{aligned}\frac{\langle\sigma|\hat{n}^z_{0,0}|\epsilon\rangle}{\langle\sigma|\hat{n}^z_{0,0}|0\rangle} &\approx \frac{c_\sigma f_{\sigma\sigma\epsilon}R^{-\Delta_\sigma} + c_{\Box\sigma}f_{\sigma,\Box\sigma,\epsilon}R^{-(\Delta_\sigma+2)} + c_{\Box^2\sigma}f_{\sigma,\Box^2\sigma,\epsilon}R^{-(\Delta_\sigma+4)} + c_{\sigma'}f_{\sigma,\sigma',\epsilon}R^{-\Delta_{\sigma'}}}{c_\sigma R^{-\Delta_\sigma} + c_{\Box\sigma}R^{-(\Delta_\sigma+2)} + c_{\Box^2\sigma}R^{-(\Delta_\sigma+4)} + c_{\sigma'}R^{-\Delta_{\sigma'}}} \\ &\approx f_{\sigma\sigma\epsilon} + \frac{c_1}{R^2} + \frac{c_2}{R^4} + O(R^{-4.77}) \approx f_{\sigma\sigma\epsilon} + \frac{c_1'}{N} + \frac{c_2'}{N^2} + O(N^{-2.38}).\end{aligned} \tag{141}$$

In the last line of Eq.(141), we change the variable from the spherical radius R to the number of Ising spins N on the fuzzy sphere. It shows that the OPE coefficients can be achieved by extrapolation $N \to \infty$.

The OPE $\sigma\sigma\epsilon$ can also be defined as $\langle\sigma|\epsilon|\sigma\rangle$ and computed using a Z_2 even operator such as $\hat{n}^x(\mathbf{\Omega})$

$$\hat{n}^x(\mathbf{\Omega}) = c_I\hat{I} + [c_\epsilon\hat{\epsilon}(\mathbf{\Omega}) + \cdots] + [c_{T_{\mu\nu}}\hat{T}_{\mu\nu}(\mathbf{\Omega}) + \cdots] + [c_{\epsilon'}\hat{\epsilon}'(\mathbf{\Omega}) + \cdots] + \cdots \tag{142}$$

where each bracket refers to a primary and its descendants (labeled by $\cdots$), with conformal dimensions of the first few lying ones to be $\Delta_I = 0$, $\Delta_\epsilon \approx 1.4126$, $\Delta_{T_{\mu\nu}} = 3$, $\Delta_{\epsilon'} \approx 3.8296$. The identity component should be subtracted, we have

$$\begin{aligned}\frac{\langle\sigma|\hat{n}^x_{0,0}|\sigma\rangle - \langle 0|\hat{n}^x_{0,0}|0\rangle}{\langle\epsilon|\hat{n}^x_{0,0}|0\rangle} &\approx \frac{c_\epsilon f_{\sigma\epsilon\sigma}R^{-\Delta_\epsilon} + c_{\square\epsilon}f_{\sigma,\square\epsilon,\sigma}R^{-(\Delta_\epsilon+2)} + c_{\epsilon'}f_{\sigma,\epsilon',\sigma}R^{-\Delta_{\epsilon'}} + c_{\square^2\epsilon}f_{\sigma,\square^2\epsilon,\sigma}R^{-(\Delta_\epsilon+4)}}{c_\epsilon R^{-\Delta_\epsilon} + c_{\square\epsilon}R^{-(\Delta_\epsilon+2)} + c_{\epsilon'}R^{-\Delta_{\epsilon'}} + c_{\square^2\epsilon}R^{-(\Delta_\epsilon+4)}} \\ &\approx f_{\sigma\sigma\epsilon} + \frac{c_1}{R^2} + \frac{c_2}{R^{2.4173}} + \frac{c_3}{R^4} + O(R^{-4.4173}) \approx f_{\sigma\sigma\epsilon} + \frac{c'_1}{N} + \frac{c'_2}{N^{1.2087}} + O(N^{-2}).\end{aligned} \tag{143}$$

Similarly, the OPE $\sigma\sigma\epsilon$ can also be computed by local spin operator $\hat{O}_\epsilon(\mathbf{\Omega})$. The finite-size scaling form is the same with different numerical factors c_α.

2. Scalar OPE coefficients: $f_{\epsilon\epsilon\epsilon}$, $f_{\sigma\sigma\epsilon'}$, $f_{\sigma'\sigma\epsilon}$, $f_{\epsilon\epsilon\epsilon'}$, $f_{\sigma'\epsilon\sigma'}$ and $f_{\sigma'\sigma\epsilon'}$ Similar to Eq. (142-143), the finite-size scaling of OPE $\epsilon\epsilon\epsilon$ reads

$$\begin{aligned}\frac{\langle\epsilon|\hat{n}^x_{0,0}|\epsilon\rangle - \langle 0|\hat{n}^x_{0,0}|0\rangle}{\langle\epsilon|\hat{n}^x_{0,0}|0\rangle} &\approx \frac{c_\epsilon f_{\epsilon\epsilon\epsilon}R^{-\Delta_\epsilon} + c_{\square\epsilon}f_{\epsilon,\square\epsilon,\epsilon}R^{-(\Delta_\epsilon+2)} + c_{\epsilon'}f_{\epsilon,\epsilon',\epsilon}R^{-\Delta_{\epsilon'}} + c_{\square^2\epsilon}f_{\epsilon,\square^2\epsilon,\epsilon}R^{-(\Delta_\epsilon+4)}}{c_\epsilon R^{-\Delta_\epsilon} + c_{\square\epsilon}R^{-(\Delta_\epsilon+2)} + c_{\epsilon'}R^{-\Delta_{\epsilon'}} + c_{\square^2\epsilon}R^{-(\Delta_\epsilon+4)}} \\ &\approx f_{\epsilon\epsilon\epsilon} + \frac{c_1}{R^2} + \frac{c_2}{R^{2.4173}} + \frac{c_3}{R^4} + O(R^{-4.4173}) \approx f_{\epsilon\epsilon\epsilon} + \frac{c'_1}{N} + \frac{c'_2}{N^{1.2087}} + O(N^{-2}).\end{aligned} \tag{144}$$

Similarly,

$$\begin{aligned}\frac{\langle\sigma|\hat{n}^z_{0,0}|\epsilon'\rangle}{\langle\sigma|\hat{n}^z_{0,0}|0\rangle} &\approx f_{\sigma\sigma\epsilon'} + \frac{c_1}{R^2} + \frac{c_2}{R^4} + O(R^{-4.77}) \approx f_{\sigma\sigma\epsilon'} + \frac{c'_1}{N} + \frac{c'_2}{N^2} + O(N^{-2.38}) \\ \frac{\langle\sigma'|\hat{n}^z_{0,0}|\epsilon\rangle}{\langle\sigma|\hat{n}^z_{0,0}|0\rangle} &\approx f_{\sigma'\sigma\epsilon} + \frac{c_1}{R^2} + \frac{c_2}{R^4} + O(R^{-4.77}) \approx f_{\sigma'\sigma\epsilon} + \frac{c'_1}{N} + \frac{c'_2}{N^2} + O(N^{-2.38}) \\ \frac{\langle\sigma'|\hat{n}^x_{0,0}|\sigma\rangle}{\langle\epsilon|\hat{n}^x_{0,0}|0\rangle} &\approx f_{\sigma'\sigma\epsilon} + \frac{c_1}{R^2} + \frac{c_2}{R^{2.4173}} + \frac{c_3}{R^4} + O(R^{-4.4173}) \approx f_{\sigma'\sigma\epsilon} + \frac{c'_1}{N} + \frac{c'_2}{N^{1.2087}} + O(N^{-2}), \\ \frac{\langle\epsilon|\hat{n}^x_{0,0}|\epsilon'\rangle}{\langle\epsilon|\hat{n}^x_{0,0}|0\rangle} &\approx f_{\epsilon\epsilon\epsilon'} + \frac{c_1}{R^2} + \frac{c_2}{R^{2.4173}} + \frac{c_3}{R^4} + O(R^{-4.4173}) \approx f_{\epsilon\epsilon\epsilon'} + \frac{c'_1}{N} + \frac{c'_2}{N^{1.2087}} + O(N^{-2})\end{aligned} \tag{145, 146}$$

In the last two equations, the identity component shouldn't be subtracted since $\langle\sigma'|\hat{I}|\sigma\rangle = \langle\epsilon'|\hat{I}|\epsilon\rangle = 0$. The numerical results are shown in Fig.**??**(a-b), (e) and can be fitted as(up to

linear term)

$$\begin{aligned}
\frac{\langle\sigma|\hat{n}^z_{0,0}|\epsilon'\rangle}{\langle\sigma|\hat{n}^z_{0,0}|0\rangle} &\approx 0.0529389 - \frac{0.35087}{N} \\
\frac{\langle\sigma'|\hat{n}^z_{0,0}|\epsilon\rangle}{\langle\sigma|\hat{n}^z_{0,0}|0\rangle} &\approx 0.0514531 - \frac{0.329505}{N} \\
\frac{\langle\sigma'|\hat{n}^x_{0,0}|\sigma\rangle}{\langle\epsilon|\hat{n}^x_{0,0}|0\rangle} &\approx 0.052771 - \frac{0.66503}{N} \\
\frac{\langle\epsilon|\hat{n}^x_{0,0}|\epsilon'\rangle}{\langle\epsilon|\hat{n}^x_{0,0}|0\rangle} &\approx 1.56597 - \frac{4.10764}{N}
\end{aligned} \tag{147}$$

where the extracted OPE coefficient are $f_{\sigma\sigma\epsilon'} \approx 0.0529389$, $f_{\sigma'\sigma\epsilon} \approx 0.0514531(\hat{n}^z), 0.052771(\hat{n}^x)$ and $f_{\epsilon\epsilon\epsilon'} \approx 1.56597$. The conformal bootstrap results are $f^{CB}_{\sigma\sigma\epsilon'} \approx 0.053012(55)$, $f^{CB}_{\sigma'\sigma\epsilon} \approx 0.057235(20)$, and $f^{CB}_{\epsilon\epsilon\epsilon'} \approx 1.5360(16)$.

Finally, we compute two OPE coefficients $f_{\sigma'\epsilon\sigma'}$ and $f_{\sigma'\sigma\epsilon'}$ that have not been computed by conformal bootstrap so far. We have,

$$\begin{aligned}
\frac{\langle\sigma'|\hat{n}^x_{0,0}|\sigma'\rangle - \langle 0|\hat{n}^x_{0,0}|0\rangle}{\langle\epsilon|\hat{n}^x_{0,0}|0\rangle} &\approx f_{\sigma'\epsilon\sigma'} + \frac{c_1}{R^2} + \frac{c_2}{R^{2.4173}} + \frac{c_3}{R^4} + O(R^{-4.4173}) \approx f_{\sigma'\epsilon\sigma'} + \frac{c'_1}{N} + \frac{c'_2}{N^{1.2087}} + O(N^{-2}) \\
\frac{\langle\sigma'|\hat{n}^z_{0,0}|\epsilon'\rangle}{\langle\sigma|\hat{n}^z_{0,0}|0\rangle} &\approx f_{\sigma'\sigma\epsilon'} + \frac{c_1}{R^2} + \frac{c_2}{R^4} + O(R^{-4.77}) \approx f_{\sigma'\sigma\epsilon'} + \frac{c'_1}{N} + \frac{c'_2}{N^2} + O(N^{-2.38}).
\end{aligned} \tag{148}$$

The numerical results are shown in Fig.**??**(f-g). The fitting results of $f_{\sigma'\epsilon\sigma'}$ are

$$\begin{aligned}
\frac{\langle\sigma'|\hat{n}^x_{0,0}|\sigma'\rangle - \langle 0|\hat{n}^x_{0,0}|0\rangle}{\langle\epsilon|\hat{n}^x_{0,0}|0\rangle} &\approx 3.17844 + \frac{30.9552}{N} \\
\frac{\langle\sigma'|(\hat{O}_\epsilon)_{0,0}|\sigma'\rangle - \langle 0|(\hat{O}_\epsilon)_{0,0}|0\rangle}{\langle\epsilon|(\hat{O}_\epsilon)_{0,0}|0\rangle} &\approx 2.97839 + \frac{5.66358}{N},
\end{aligned}$$

And the result of $f_{\sigma'\sigma\epsilon'}$ is

$$\frac{\langle\sigma'|\hat{n}^z_{0,0}|\epsilon'\rangle}{\langle\sigma|\hat{n}^z_{0,0}|0\rangle} \approx 1.29367 - \frac{3.05227}{N}.$$

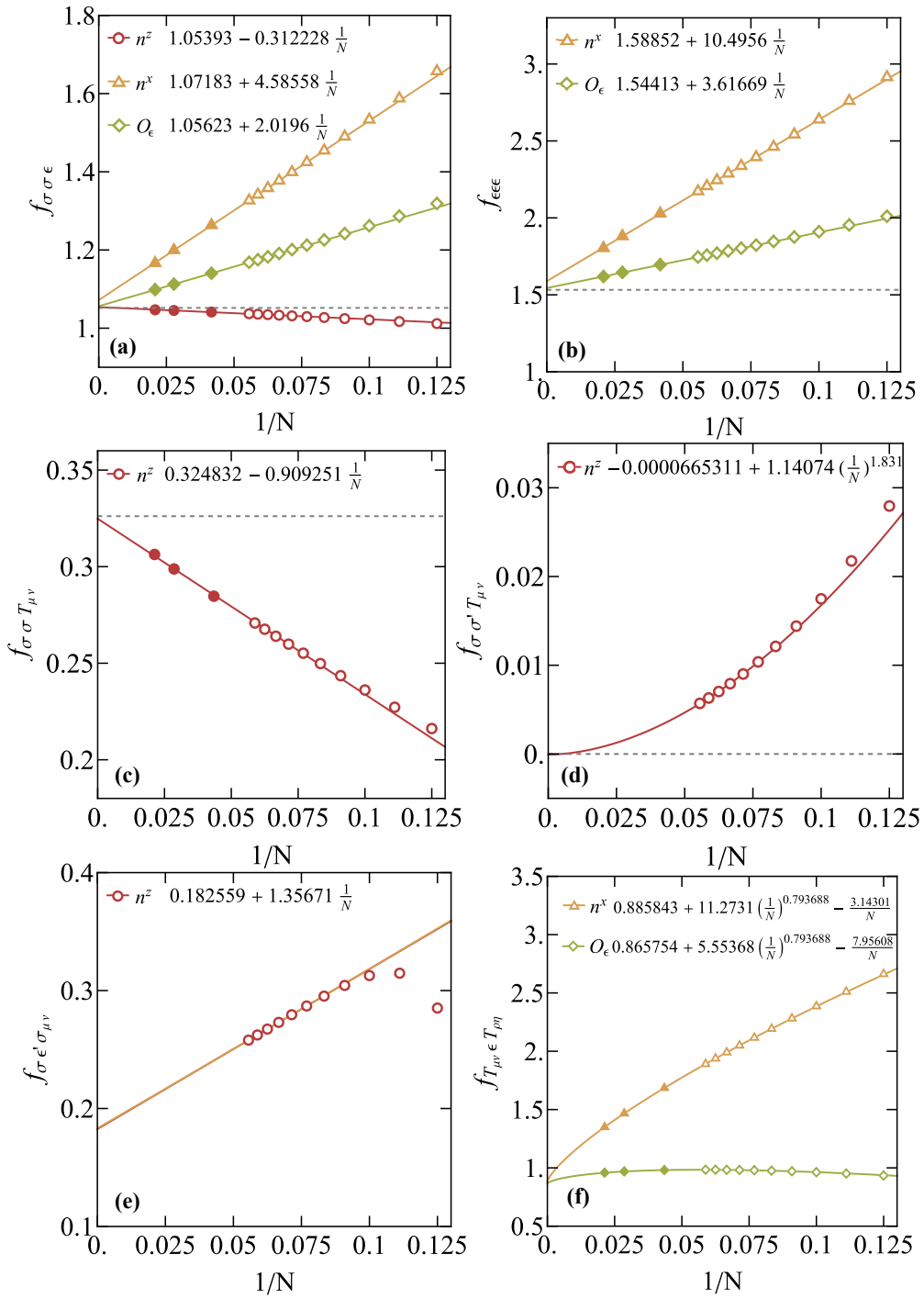

FIG. 9. **OPE coefficients of primary operators**. (a-b) Two representative OPE coefficients involving three scalar primaries $f_{\sigma\sigma\epsilon}$ and $f_{\epsilon\epsilon\epsilon}$, obtained from the finite-size extrapolation via spin operator $n^z(\mathbf{\Omega})$ (red), $n^x(\mathbf{\Omega})$ (yellow) and $O_\epsilon(\mathbf{\Omega})$ (green) (see main text). (c-d) Two representative OPE coefficients involving energy-momentum tensor $f_{\sigma\sigma T_{\mu\nu}}, f_{\sigma'\sigma T_{\mu\nu}}$ by using $n^z(\mathbf{\Omega})$ operator. The dashed line in (a-d) is the value from conformal bootstrap. (e-f) Two representative OPE coefficients $f_{\sigma\epsilon'\sigma_{\mu\nu}}, f_{T_{\mu\nu}\epsilon T_{\mu\nu}}$ that are not known in conformal bootstrap calculation. In all figures only the data points on largest six sizes are used in the fitting. In (a-c) and (f), larger sizes up to $N = 48$ are available by the DMRG method which are labeled by solid symbols.

TABLE II. List of OPE coefficients of primary operators obtained on the fuzzy sphere. The primary operators in consideration have scaling dimensions $\Delta_\sigma \approx 0.51815$, $\Delta_\epsilon \approx 1.4126$, $\Delta_{\epsilon'} \approx 3.8297$, $\Delta_{\sigma'} \approx 5.2906$, $\Delta_{T_{\mu\nu}} = 3$, and $\Delta_{\sigma_{\mu\nu}} \approx 4.1803$. The conformal bootstrap (CB) data is from Ref. [45], where some of unavailable data is labeled by 'NA'. We note that our convention for $f_{T_{\mu\nu}\epsilon T_{\rho\eta}}$ is $f_{T_{\mu\nu}\epsilon T_{\rho\eta}} = \frac{1}{\sqrt{4\pi}} \int d\mathbf{\Omega}\, \langle T_{\mu\nu}, m=0 | \hat{\epsilon}(\mathbf{\Omega}) | T_{\rho\eta}, m=0 \rangle$ [**?**].

Operators	Spin	Z_2	$f_{\alpha\beta\gamma}$ (Fuzzy Sphere)	$f_{\alpha\beta\gamma}$ (CB)
σ	0	$-$	$f_{\sigma\sigma\epsilon} \approx 1.0539(18)$	$f_{\sigma\sigma\epsilon} \approx 1.0519$
ϵ	0	$+$	$f_{\epsilon\epsilon\epsilon} \approx 1.5441(23)$	$f_{\epsilon\epsilon\epsilon} \approx 1.5324$
ϵ'	0	$+$	$f_{\sigma\sigma\epsilon'} \approx 0.0529(16)$	$f_{\sigma\sigma\epsilon'} \approx 0.0530$
			$f_{\epsilon\epsilon\epsilon'} \approx 1.566(68)$	$f_{\epsilon\epsilon\epsilon'} \approx 1.5360$
σ'	0	$-$	$f_{\sigma'\sigma\epsilon} \approx 0.0515(42)$	$f_{\sigma'\sigma\epsilon} \approx 0.0572$
			$f_{\sigma'\sigma\epsilon'} \approx 1.294(51)$	NA
			$f_{\sigma'\epsilon\sigma'} \approx 2.98(13)$	NA
$T_{\mu\nu}$	2	$+$	$f_{\sigma\sigma T} \approx 0.3248(35)$	$f_{\sigma\sigma T} \approx 0.3261$
			$f_{\sigma'\sigma T} \approx -0.00007(96)$	$f_{\sigma'\sigma T} = 0$
			$f_{\epsilon\epsilon T} \approx 0.8951(35)$	$f_{\epsilon\epsilon T} \approx 0.8892$
			$f_{T\epsilon T} \approx 0.8658(69)$	NA
$\sigma_{\mu\nu}$	2	$-$	$f_{\sigma\epsilon\sigma_{\mu\nu}} \approx 0.400(33)$	$f_{\sigma\epsilon\sigma_{\mu\nu}} \approx 0.3892$
			$f_{\sigma\epsilon'\sigma_{\mu\nu}} \approx 0.18256(69)$	NA

IV. MORE APPLICATIONS

A. Phase transitions

1. 3-State Potts universality

Drawing upon the previous Ising model [25] with a global Z_2 symmetry, we consider interacting fermions with three flavors to achieve the full S_3 permutation symmetry. We construct three-component fermions living on the fuzzy sphere. The system is characterized by a continuous Hamiltonian:

$$H=\int d\Omega_a d\Omega_b U\left(\Omega_{ab}\right)\left[n_0\left(\Omega_a\right)n_0\left(\Omega_b\right)-n_z\left(\Omega_a\right)n_z^\dagger\left(\Omega_b\right)\right]-h\int d\Omega\left[n_x\left(\Omega\right)+n_x^\dagger\left(\Omega\right)\right] \quad (149)$$

where $\Omega=(\theta,\psi)$ is spatial coordinates on a sphere with radius R, density operator reads $n_\alpha(\Omega)=\psi^\dagger(\Omega)S_\alpha\psi(\Omega)$, and S_α is defined in $Q=3$ local Hilbert space

$$S_0=\begin{pmatrix}1&0&0\\0&1&0\\0&0&1\end{pmatrix},S_z=\begin{pmatrix}1&0&0\\0&e^{i\frac{2\pi}{3}}&0\\0&0&e^{i\frac{4\pi}{3}}\end{pmatrix},S_x=\begin{pmatrix}0&0&1\\1&0&0\\0&1&0\end{pmatrix}. \quad (150)$$

The interaction term $U\left(\Omega_{ab}\right)=\frac{g_0}{R^2}\delta\left(\Omega_{ab}\right)+\frac{g_1}{R^4}\nabla^2\delta\left(\Omega_{ab}\right)$ is taken to be local and short-ranged, ensuring that the phase transition is described by a local theory. After projecting to the lowest Landau level (LLL), the second quantized Hamiltonian can be derived in the following form:

$$H=\sum_{m_1m_2m_3m_4}V_{m_1m_2m_3m_4}\left[\left(\boldsymbol{c}_{m_1}^\dagger\boldsymbol{c}_{m_4}\right)\left(\boldsymbol{c}_{m_2}^\dagger\boldsymbol{c}_{m_3}\right)-\left(\boldsymbol{c}_{m_1}^\dagger S_z\boldsymbol{c}_{m_4}\right)\left(\boldsymbol{c}_{m_2}^\dagger S_z^\dagger\boldsymbol{c}_{m_3}\right)\right]-h\sum_m\boldsymbol{c}_m^\dagger\left(S_x+S_x^\dagger\right)\boldsymbol{c}_m \quad (151)$$

where $\boldsymbol{c}_m^\dagger=\left(c_{m0}^\dagger,c_{m1}^\dagger,c_{m2}^\dagger\right)$ is the fermion creation operator on the m_{th} Landau orbital, and V_{m_1,m_2,m_3,m_4} is associated with Haldane pseudopotential V_l with following form:

$$V_{m_1m_2m_3m_4}=\sum_l V_l(4s-2l+1)\begin{pmatrix}s&s&2s-l\\m_1&m_2&-m_1-m_2\end{pmatrix}\begin{pmatrix}s&s&2s-l\\m_4&m_3&-m_4-m_3\end{pmatrix}\delta_{m_1+m_2,m_3+m_4}, \quad (152)$$

where $\begin{pmatrix}j_1&j_2&j_3\\m_1&m_2&m_3\end{pmatrix}$ is the Wigner 3j symbol. In this paper, we will only consider ultra-local interactions U in real space, which corresponds to non-zero Haldane pseudopotentials V_0 and V_1, and we set $V_0=1$.

In 2D, the Potts model exhibits two families of CFTs with the same global symmetry, regarding the critical and tricritical branches, respectively. For the $D = 3$ Potts model, the first-order phase transition is expected to appear for $Q > Q_c(3)$ as shown in Fig. 10 [55–58], but the critical value $Q_c(D = 3)$ is not exactly known. Historically, the critical value $Q_c(3)$ has been estimated by various methods, such as $Q_c(3) \approx 2.7$ from the ϵ-expansion [55], $Q_c(3) \approx 2.2$ from the Kadanoff variational renormalization group [56], $2 < Q_c(3) < 3$ from various Monte Carlo calculations [59–61] and $Q_c(3) \approx 2.11$ from the non-perturbative renormalization group [57]. The Monte Carlo simulations partially support the above estimations [62–64] and the tensor renormalization group simulations , where the first-order transition is observed in the 3D $Q = 3$-state Potts model. Moreover, based on a recent numerical bootstrap study [65], fixing $Q = 3$, the critical space-time dimension separating the continuous and first-order transition is around $D_c \approx 2.6$. These results indicate that in the physical parameter space (see Fig. 10), the 3D 3-state Potts model ($D = 3, Q = 3$) is sitting close to the phase boundary. Additionally, the conformal fixed points merge-and-annihilate picture is also supported by the calculation based on the non-perturbative renormalization group in higher dimensions [56–58]. Notably, Recent field-theoretic developments further clarify this picture: the work of Wiese and Jacobsen [66] confirms that the non-perturbative RG fixed point persists deep into the first-order region, reinforcing the interpretation of complex fixed points as a universal feature of discontinuous transitions. Inspired by these facts, a natural conjecture is a first-order transition in the 3D 3 state Potts model can also be described by the complex CFT, akin to the 2D ($Q > 4$)-state Potts model.

2. $O(N)$ Wilson-Fisher universality

A natural generalization of the 3D Ising universality class is the $O(N)$ Wilson-Fisher (WF) universality (e.g. see a review [4]), where the Ising corresponds to $N = 1$. Similar to the Ising model, the $O(N)$ model describes an order-disorder transition, in which the ordered phase exhibits spontaneous symmetry breaking of $O(N)$. In nature, the $O(2)$ WF (also called XY) universality class describes the superfluid-to-normal fluid transition in helium-4, while the $O(3)$ WF universality class describes the Heisenberg ferromagnetic phase transition.

The general guiding principle for designing fuzzy sphere models is to ensure that the global symmetry and ('t Hooft) anomaly of the fuzzy sphere model match those of the target

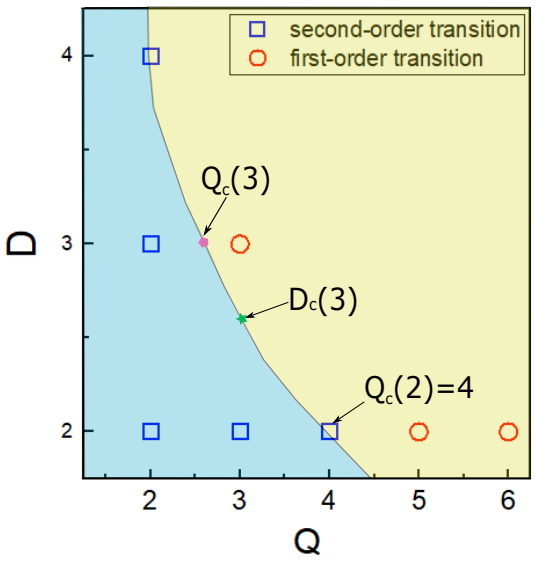

$Q_c(3)$	Ref.
2.7	ϵ-exp [55]
2.2	RG [56]
2.21	MC [59]
2.45	MC [60]
2.65	MC [61]
2.15	SCOZA [67]
2.11	RG[57]
2.35	MC [68]
$D_c(3)$	Ref.
2.6	CB [65]

FIG. 10. (Left panel) The nature of Potts transition depends on space-time dimension D and spin component Q [55–60, 67, 68], where the continuous transition exists for $Q \leq Q_c, D \leq D_c$. Here Q_c, D_c are the largest critical values for which the Potts transition is continuous. (Right panel) The estimated values of $Q_c(D=3)$ and $D_c(Q=3)$ from various literature.

universality class. Since the $O(N)$ WF universality class does not exhibit any anomaly, the corresponding fuzzy sphere model must also preserve $O(N)$ symmetry and remain anomaly-free. For example, Ref. [26] investigated a $O(3)$ WF model, which also involves four fermion flavors but with two fermions per Landau orbital. We consider a real-space Hamiltonian:

$$H_{\text{int}} = \int d\vec{\Omega}_{a,b}\Big[U_0 n(\vec{\Omega}_a)n(\vec{\Omega}_b) + U_2\vec{n}_1(\vec{\Omega}_a)\cdot\vec{n}_2(\vec{\Omega}_b) - U_1(\vec{n}_1(\vec{\Omega}_a)\cdot\vec{n}_1(\vec{\Omega}_b) + \vec{n}_2(\vec{\Omega}_a)\cdot\vec{n}_2(\vec{\Omega}_b))\Big] - h\int d\vec{\Omega}\hat{\mathbf{\Psi}}^\dagger\tau^x\sigma^0\hat{\mathbf{\Psi}},$$

where the local density operator of layer-τ is $\vec{n}_\tau(\vec{\Omega}) = (n^x_\tau, n^y_\tau, n^z_\tau) = \psi^\dagger_\tau(\vec{\Omega})\vec{\sigma}\psi_\tau(\vec{\Omega})$ and the total density is $n(\vec{\Omega}) = \mathbf{\Psi}^\dagger(\vec{\Omega})\mathbf{\Psi}(\vec{\Omega})$. For simplicity, we consider the potentials to be short-ranged interactions $\delta(\vec{\Omega}_1 - \vec{\Omega}_2)$ and $\nabla^2\delta(\vec{\Omega}_1 - \vec{\Omega}_2)$. The transverse field strength h controls tunneling effect between two different layers.

After verifying the emergent conformal symmetry, we further compare scaling dimensions of the identified primary operators with the existing data from various methods [11, 70, 71]. As listed the relevant primary operators that we have identified in Tab. III, overall we

find a reasonable agreement with numerical bootstrap [11, 70] and Monte Carlo data [71], e.g. the averaged discrepancy from the bootstrap data is less than 1%. Despite of the small discrepancy, the precision is still sufficiently high to further increase the confidence that the universality class of the transition falls into the 3D Wilson-Fisher O(3) type. In particular, these data are crucial to understand the physics of O(3) critical point. For instance, the lowest rank-4 symmetric tensor operator t_4 corresponds to the anisotropic cubic perturbation. This operator is dangerously relevant, according to the existing numerical computation [69, 70]. Our calculation confirms its relevance $\Delta_{t_4} \approx 2.961(12)$. Here we notice that the finite-size effect of t_4 is strong, since the finite-size value of its scaling dimension

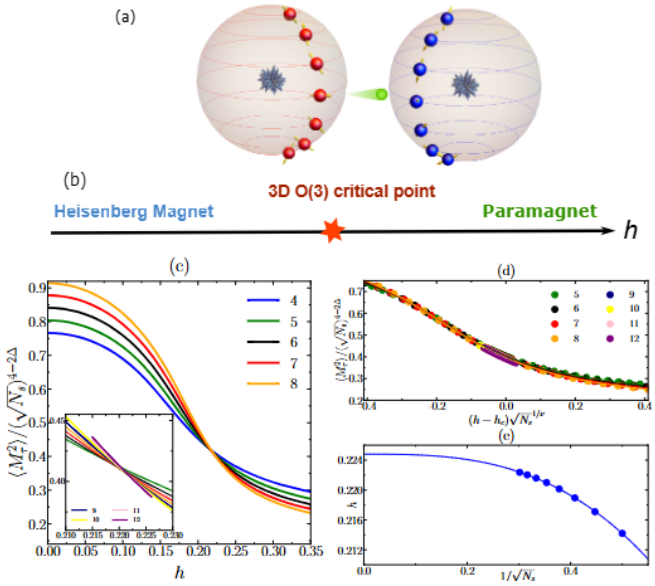

FIG. 11. (a) Sketches of the bilayer fuzzy sphere model: Interacting fermions move on a fuzzy sphere bilayer; and the fermion is able to tunnel between two layers. (b) A schematic plot of phase diagram with a critical point separating a paramagnet from a symmetry breaking Heisenberg magnet. (c) Finite size scaling of order parameter $\langle M^2_{1(2)}\rangle/N_s^{2-\Delta_\phi}$, where $\Delta_\phi = 0.519$ is the scaling dimension of the O(3) vector field relating to the critical exponent $\eta = 2\Delta_\phi - 1$. $N_s = 2s + 1$ is the number of Landau orbitals (i.e. Heisenberg spins), which relates to the length scale radius as $R \sim \sqrt{N_s}$. (d) The data collapse of the rescaled order parameter according to $f((h - h_c)L^{1/\nu})$ with $\nu = 1/(3 - \Delta_s)$ and $\Delta_s \approx 1.595$, where h_c is a free fitting parameter. The best fit gives $h_c \approx 0.225$. (e) Finite size scaling of crossing points by a finite-size pair $(N_s, N_s + 1)$ gives rise to an extrapolated value $h_c \approx 0.2248 \pm 0.0001$.

flows from irrelevant to relevant. This strong flow results from the influence of high-level irrelevant fields. To resolve this problem, much larger system sizes are needed, which is beyond the current computational ability.

3. Lee-Yang universality

The origin of the Lee-Yang CFT and its role in our understanding of order–disorder phase transitions is a remarkable chapter in theoretical physics. The universal, long-distance physics, of the LY edge singularity is captured by the following field theory action:

$$S = \int d^d x [\frac{1}{2}(\partial\phi)^2 + \frac{i\lambda}{3!}\phi^3] \tag{153}$$

The coupling $i\lambda$ is purely imaginary, rendering the theory non-unitary while preserving stability by avoiding runaway directions.

The current state-of-the-art five-loop ϵ-expansion estimates yield $\Delta_\phi = 0.215(1)$ for $D = 3$ this value lies below the unitarity bound. The operator ϕ^2 is redundant with via the equations of motion $\partial^2\phi \sim \phi^2$. Next, as in any local CFT, the Lee-Yang has an energy momentum tensor: a spin-two primary operator of dimension $\Delta_T = 3$. The next primary operators in the spectrum are a scalar operator ϕ^3 and a spin $\ell = 4$ operator $C_{\mu\nu\rho\sigma}$, which have estimated dimensions above three – indeed $\Delta_{\phi^3} = 5.0(1)$ and $\Delta_C = 4.75(1)$.

TABLE III. Low-lying primary operators identified via state-operator correspondence on the fuzzy sphere. We only take the first three digits from the data in literature.

	ϕ	t_2	s	t_3	t_4
$\epsilon-$exp[69]	0.510	1.232	1.610	-	2.911
large-N[69]	0.499	1.339	1.301	-	3.447
Bootstrap[70]	0.519	1.209	1.595	2.039	< 2.991
MC[71]	0.519	1.210	1.594	2.039	2.986
Fuzzy sphere	0.524	1.211	1.588	2.028	2.961

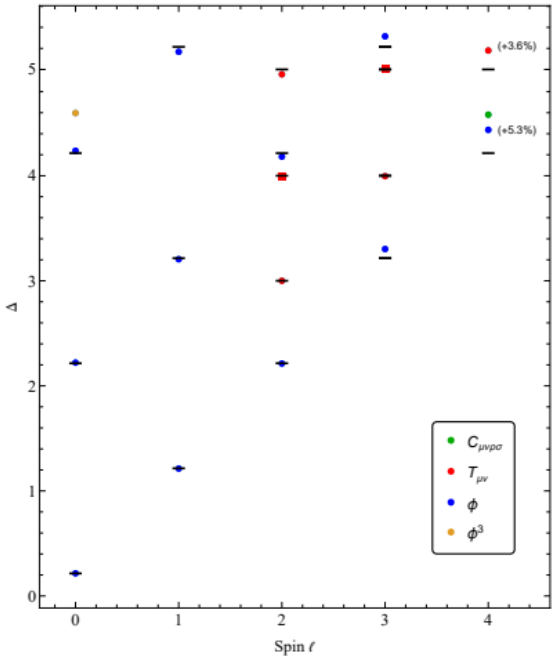

FIG. 12. Operator spectra of Lee-Yang model on the fuzzy sphere (with finite-size correction).

The hamiltonian on fuzzy sphere will be

$$H_{LY} = H_{Ising} + ig_z \int d\Omega n^z(\Omega) \tag{154}$$

The CFT data is shown in Fig. 12. The results match the expectation quite well (The proper finite-size scaling is necessary).

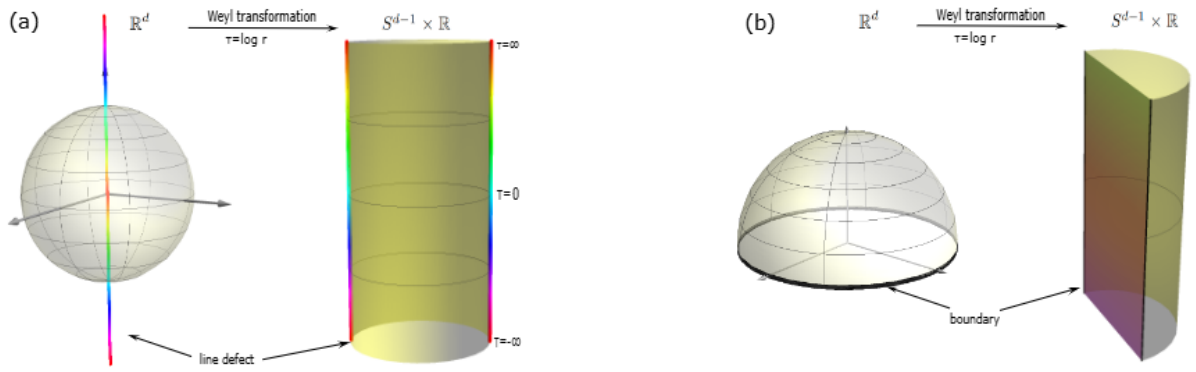

FIG. 13. **Schematic plot of the defect and boundary in 3D**. (a) The line defect and (b) the boundary before and after the Weyl transformation.

B. Defects/Boundaries CFT

Defects and boundaries are ubiquitous in the real world, and in the realm of critical phenomena, they can give rise to new physics, including distinct defect and boundary universality classes. A well-known example of a defect in critical phenomena is the Kondo effect, the study of which played a pivotal role in the development of RG theory, revolutionizing modern physics.

Introducing a defect or boundary into a bulk CFT can trigger an RG flow toward a nontrivial IR fixed point on the defect or boundary, leading to a defect CFT (dCFT) [15, 72] or a boundary CFT (bCFT) [73–75]. The dCFT [76] exhibits a rich array of new physical phenomena. First, a given bulk CFT can host multiple defect universality classes, making it particularly interesting to explore the landscape of defect fixed points. For each defect fixed point, the original conformal symmetry of the bulk is broken down to a smaller conformal symmetry on the defect. New operators exist on the defect, which can still be classified into primaries and descendants under the defect conformal group. Moreover, there is a nontrivial interplay between the defect and the bulk, allowing for interesting correlation functions between bulk and defect operators. Finally, RG monotonicity theorems also apply to defect RG flows; for instance, the g-theorem of the line defect has been proven for bulk CFTs in various dimensions [77–79].

Similar to bulk CFTs, it is natural to study dCFTs in R^d. Then by applying a Weyl transformation, one can map the theory onto the cylinder $S^{d-1} \times R$, which again benefits from the advantages of the fuzzy sphere scheme. In particular, the state-operator correspondence

remains valid for dCFTs. As shown in Fig. 13, a line defect in R^d is mapped to $S^{d-1} \times R$, where $0+1$D impurities are located at the north and south poles. Similarly, a CFT with a boundary in R^d is mapped to a setup where the spatial dimensions reside on a hemisphere rather than a full sphere. One can also consider defect-changing operators, which sit at the junction between two different types of semi-infinite line defects. On $S^{d-1} \times R$, this corresponds to placing different types of impurities at the north and south poles.

The simplest example of a conformal defect is the pinning field defect [80] in the 3D Ising CFT, where a Ising Z_2-breaking magnetic field is applied along a line defect. In field theory, this corresponds to turning on the σ field on the 1D line defect, which is relevant ($\Delta_\sigma < 1$) and therefore induces an RG flow to a nontrivial IR defect fixed point. In the fuzzy sphere model, this line defect can be realized by adding impurity terms at north and south pole,

$$h_{\mathrm{N}} n^z(\mathbf{x} = \text{North Pole}) + h_{\mathrm{S}} n^z(\mathbf{x} = \text{South Pole}), \tag{155}$$

to the original Hamiltonian. The eigenstates of this Hamiltonian are in one-to-one correspondence with the operators of the dCFT. Interestingly, different choices of impurity terms correspond to different types of operators: setting $h_{\mathrm{N}} = h_{\mathrm{S}}$ yields defect operators, $h_{\mathrm{N}} = -h_{\mathrm{S}}$ gives defect-changing operators, and ($h_{\mathrm{N}} \neq 0, h_{\mathrm{S}} = 0$) produces defect-creation operators. Ref. [32] observed the state-operator correspondence for defect operators, explicitly demonstrated the defect conformal invariance, and obtained the scaling dimensions of several defect primary operators as well as bulk-defect OPE coefficients. Moreover, Ref. [33] computed the g-function using wavefunction overlap, obtaining $g = 0.602(2)$, a result later reproduced by the rigorous bootstrap approach [81]. In the same work, the authors also studied defect-creation and defect-changing operators, demonstrating that spontaneous Ising Z_2 breaking is unstable on the line defect of the 3D Ising CFT. Additionally, Ref. [82] calculated the cusp anomalous dimension for the Ising pinning field line defect.

Shifting focus from defects to boundaries, Refs. [34, 35] studied the bCFT of the 3D Ising model on the fuzzy hemisphere. The key idea is that one can construct a fuzzy hemisphere by removing half of the Landau orbitals of the LLL. The authors investigated both the normal boundary (which explicitly breaks Z_2 symmetry) and the ordinary boundary (which preserves Z_2 symmetry). The emergent boundary conformal symmetry was once again demonstrated through the state-operator correspondence, along with results for boundary primary operators and bulk-boundary OPE coefficients. Moreover, Ref. [34] computed the

boundary central charge, an RG-monotonic quantity governing the boundary RG flow [83]. Additionally, the same work reported an intriguing connection between the bCFT operator spectrum and the bulk entanglement spectrum in Landau orbital space.

C. F-Function: 3D Analog of the Central Charge in 2D CFT

RG theory is fundamental for understanding scale-dependent behaviors in critical phenomena. Since RG transformations integrate out short-distance degrees of freedom, a key feature of RG flow is its irreversibility—certain complexity measures, such as the number of degrees of freedom, monotonically decrease along the flow. The first established RG irreversibility theorem is Zamolodchikov's c-theorem in 2D [84]. The c-theorem states that a c-function, associated with the central charge of 2D CFTs at RG fixed points, monotonically decreases under RG flow. The 2D c-theorem was later conjectured by Cardy [85] to generalize to the a-theorem in 4D, which was subsequently proven by Komargodski and Schwimmer [86]. Both the 2D central charge and the 4D a-function are related to the conformal anomaly and can be computed from stress tensor correlators.

In 3D, a similar RG irreversibility theorem exists—the F-theorem. In this case, the RG monotonic F-function is defined through the partition function on the three-sphere S^3 [87]. Mapping S^3 to $\mathbb{R}^3$ via a conformal transformation, the F-function appears in the entanglement entropy—specifically, it corresponds to the subleading term in addition to the conventional entanglement area law [88]. The entanglement version of the F-theorem has been proven using entanglement subadditivity [89]. Unlike the c- and a-functions, the F-function is inherently non-local, as it is not related to the conformal anomaly and cannot be computed from the correlators of any local operators. Instead, it must be extracted from a non-local quantity on a conformally flat manifold, such as the entanglement entropy in $\mathbb{R}^3$ or $S^2 \times \mathbb{R}$ (but not on T^3 or $T^2 \times \mathbb{R}$). This makes the F-function particularly challenging to compute.

The fuzzy sphere offers several unique advantages for computing the F-function [31]. On the fuzzy sphere, one can consider the entanglement entropy of a real-space entanglement cut at a latitude parameterized by θ on a sphere of radius R:

$$S_A(\theta) = -\mathrm{Tr}(\rho_A \ln \rho_A) = \frac{\alpha R}{\delta} \sin\theta - F, \tag{156}$$

where δ is a UV regulator. The first term represents the entanglement area law, while the second term corresponds to the F-function. Since the space is continuous, we can define the cylinder-renormalized entanglement entropy [90]:

$$\mathcal{F}_C(R,\theta_0) \equiv (\tan\theta\,\partial_\theta - 1)S_A(\theta)\Big|_{R,\theta_0}. \tag{157}$$

In the thermodynamic limit, where $R\sin\theta_0 \to \infty$, $\mathcal{F}_C(R,\theta_0)$ approaches F at the IR fixed point.

Following this strategy, Ref. [31] reported the first non-perturbative computation of the F-function for the 3D Ising CFT, yielding $F_{\text{Ising}} = 0.0612(5)$. This value is slightly smaller than the F-function of a free real scalar, $F_{\text{free}} = \frac{\log 2}{8} - \frac{3\zeta(3)}{16\pi^2} \approx 0.0638$ [91], in agreement with the F-theorem. The result is also very close to predictions from the $4-\epsilon$ expansion, which gives $F_{\text{Ising}} \approx 0.0610$ [92] and $F_{\text{Ising}} \approx 0.0623$ [93, 94].

[1] J. Cardy, *Scaling and Renormalization in Statistical Physics* (Cambridge University Press, Cambridge, England, 1996).

[2] S. Sachdev, *Quantum Phase Transitions*, 2nd ed. (Cambridge University Press, 2011).

[3] M. Henkel, *Conformal invariance and critical phenomena* (Springer Science & Business Media, 1999).

[4] A. Pelissetto and E. Vicari, Physics Reports **368**, 549 (2002).

[5] S.-K. Ma, *Modern Theory Of Critical Phenomena (1st ed.)*. (Routledge., 2001).

[6] K. G. Wilson and J. Kogut, Physics Reports **12**, 75 (1974).

[7] A. M. Polyakov, JETP Lett. **12**, 381 (1970).

[8] A. Belavin, A. Polyakov, and A. Zamolodchikov, Nuclear Physics B **241**, 333 (1984).

[9] D. S. Philippe Francesco, Pierre Mathieu, *Conformal Field Theory*, Graduate Texts in Contemporary Physics (Springer New York, NY, 1997).

[10] R. Rattazzi, V. S. Rychkov, E. Tonni, and A. Vichi, Journal of High Energy Physics **2008**, 031 (2008).

[11] D. Poland, S. Rychkov, and A. Vichi, Rev. Mod. Phys. **91**, 015002 (2019).

[12] S. Rychkov and N. Su, Rev. Mod. Phys. **96**, 045004 (2024).

[13] M. Weigel and W. Janke, Europhysics Letters (EPL) **51**, 578 (2000).

[14] Y. Deng and H. W. J. Blöte, Phys. Rev. Lett. **88**, 190602 (2002).

[15] M. Billó, M. Caselle, D. Gaiotto, F. Gliozzi, M. Meineri, and R. Pellegrini, Journal of High Energy Physics **2013**, 55 (2013), arXiv:1304.4110 [hep-th].

[16] C. Cosme, J. M. V. P. Lopes, and J. Penedones, Journal of High Energy Physics **2015**, 22 (2015), arXiv:1503.02011 [hep-th].

[17] J. L. Cardy, Journal of Physics A: Mathematical and General **17**, L385 (1984).

[18] J. L. Cardy, Journal of Physics A: Mathematical and General **18**, L757 (1985).

[19] H. W. J. Blöte, J. L. Cardy, and M. P. Nightingale, Phys. Rev. Lett. **56**, 742 (1986).

[20] I. Affleck, in *Current Physics–Sources and Comments*, Vol. 2 (Elsevier, 1988) pp. 347–349.

[21] A. Milsted and G. Vidal, Phys. Rev. B **96**, 245105 (2017), arXiv:1706.01436 [cond-mat.str-el].

[22] Y. Zou, A. Milsted, and G. Vidal, Phys. Rev. Lett. **121**, 230402 (2018).

[23] R. C. Brower, G. T. Fleming, and H. Neuberger, Physics Letters B **721**, 299 (2013),

arXiv:1212.6190 [hep-lat].

[24] R. C. Brower, G. T. Fleming, A. D. Gasbarro, D. Howarth, T. G. Raben, C.-I. Tan, and E. S. Weinberg, Phys. Rev. D **104**, 094502 (2021), arXiv:2006.15636 [hep-lat].

[25] W. Zhu, C. Han, E. Huffman, J. S. Hofmann, and Y.-C. He, Phys. Rev. X **13**, 021009 (2023).

[26] C. Han, L. Hu, and W. Zhu, Phys. Rev. B **110**, 115113 (2024).

[27] A. Lauchli, https://scgp.stonybrook.edu/video/video.php?id=6221.

[28] Z. Zhou, L. Hu, W. Zhu, and Y.-C. He, Phys. Rev. X **14**, 021044 (2024).

[29] L. Hu, Y.-C. He, and W. Zhu, Phys. Rev. Lett. **131**, 031601 (2023).

[30] C. Han, L. Hu, W. Zhu, and Y.-C. He, Phys. Rev. B **108**, 235123 (2023).

[31] L. Hu, Y. C. He, and W. Zhu, arXiv e-prints , arXiv:2401.17362 (2024), arXiv:2401.17362 [cond-mat.str-el].

[32] L. Hu, Y.-C. He, and W. Zhu, Nat. Commun. **15**, 9013 (2024).

[33] Z. Zhou, D. Gaiotto, Y.-C. He, and Y. Zou, arXiv e-prints , arXiv:2401.00039 (2023), arXiv:2401.00039 [hep-th].

[34] Z. Zhou and Y. Zou, SciPost Physics **18**, 31 (2025).

[35] M. Dedushenko, Ising bcft from fuzzy hemisphere (2024), arXiv:2407.15948 [hep-th].

[36] Z. Zhou and Y.-C. He, , arXiv.2410.00087 (2024), arXiv:2410.00087 [hep-th].

[37] F. D. M. Haldane, Phys. Rev. Lett. **51**, 605 (1983).

[38] J. Madore, Classical and Quantum Gravity **9**, 69 (1992).

[39] T. T. Wu and C. N. Yang, Nuclear Physics B **107**, 365 (1976).

[40] The spin degree of freedom should be thought as a pseudospin as it does not couple to the Zeeman field of the magnetic monopole.

[41] S. L. Sondhi, A. Karlhede, S. A. Kivelson, and E. H. Rezayi, Phys. Rev. B **47**, 16419 (1993).

[42] S. M. Girvin, Physics Today **53**, 39 (2000).

[43] M. R. Douglas and N. A. Nekrasov, Reviews of Modern Physics **73**, 977 (2001), arXiv:hep-th/0106048 [hep-th].

[44] M. Hasenbusch, Phys. Rev. B **82**, 174433 (2010).

[45] D. Simmons-Duffin, J. High Energ. Phys. **2017**, 86.

[46] D. Berkowitz and G. Fleming, arXiv e-prints , arXiv:2110.12109 (2021), arXiv:2110.12109 [hep-lat].

[47] The conformal multiplet of a conserved operator is called a short multiplet.

[48] We have targeted the lowest 100 eigenstates using ED without explicitly imposing the value of ℓ, and we only looked at states with $\ell \leq 4$ which roughly contains 70 states.

[49] To recall, the UV particle-hole symmetry becomes the spacetime parity symmetry of the IR CFT.

[50] J. Polchinski, Nuclear Physics B **303**, 226 (1988).

[51] Strictly speaking, virial current refers to an operator with scaling dimension $\Delta = 2$. If such an operator exists, one may have a theory that is scale-invariant but not conformal-invariant.

[52] S. Meneses, J. Penedones, S. Rychkov, J. M. Viana Parente Lopes, and P. Yvernay, Journal of High Energy Physics **2019**, 115 (2019), arXiv:1802.02319 [hep-th].

[53] A. Dymarsky, F. Kos, P. Kravchuk, D. Poland, and D. Simmons-Duffin, Journal of High Energy Physics **2018**, 164 (2018), arXiv:1708.05718 [hep-th].

[54] A. M. Ferrenberg, J. Xu, and D. P. Landau, Phys. Rev. E **97**, 043301 (2018).

[55] F. Y. Wu, Rev. Mod. Phys. **54**, 235 (1982).

[56] B. Nienhuis, E. K. Riedel, and M. Schick, Phys. Rev. B **23**, 6055 (1981).

[57] C. A. Sánchez-Villalobos, B. Delamotte, and N. Wschebor, Phys. Rev. E **108**, 064120 (2023).

[58] K. E. Newman, E. K. Riedel, and S. Muto, Phys. Rev. B **29**, 302 (1984).

[59] G. Barkema and J. de Boer, Phys. Rev. A **44**, 8000 (1991).

[60] J. Lee and J. M. Kosterlitz, Phys. Rev. B **43**, 1268 (1991).

[61] F. Gliozzi, Phys. Rev. E **66**, 016115 (2002).

[62] S. J. K. Jensen and O. G. Mouritsen, Phys. Rev. Lett. **43**, 1736 (1979).

[63] H. W. J. Blöte and R. H. Swendsen, Phys. Rev. Lett. **43**, 799 (1979).

[64] W. Janke and R. Villanova, Nuclear Physics B **489**, 679 (1997).

[65] S. M. Chester and N. Su, Upper critical dimension of the 3-state potts model (2022), arXiv:2210.09091 [hep-th].

[66] K. J. Wiese and J. L. Jacobsen, JHEP **05**, 092, arXiv:2311.01529 [hep-th].

[67] S. Grollau, M. Rosinberg, and G. Tarjus, Physica A: Statistical Mechanics and its Applications **296**, 460 (2001).

[68] A. K. Hartmann, Phys. Rev. Lett. **94**, 050601 (2005).

[69] J. Henriksson, Physics Reports **1002**, 1 (2023), the critical O(N) CFT: Methods and conformal data.

[70] S. M. Chester, W. Landry, J. Liu, D. Poland, D. Simmons-Duffin, N. Su, and A. Vichi, Phys.

Rev. D **104**, 105013 (2021).

[71] M. Hasenbusch, Phys. Rev. B **107**, 024409 (2023).

[72] M. Billò, V. Gonçalves, E. Lauria, and M. Meineri, Journal of High Energy Physics **2016**, 91 (2016), arXiv:1601.02883 [hep-th].

[73] J. L. Cardy, Nuclear Physics B **240**, 514 (1984).

[74] J. L. Cardy, Nuclear Physics B **324**, 581 (1989).

[75] J. L. Cardy and D. C. Lewellen, Physics Letters B **259**, 274 (1991).

[76] The general properties of defects and boundaries are similar, and a boundary can be viewed as a special type of defect. Thus, in general descriptions, we will simply refer to defects, with the understanding that the discussion also applies to boundaries.

[77] I. Affleck and A. W. W. Ludwig, Phys. Rev. Lett. **67**, 161 (1991).

[78] G. Cuomo, Z. Komargodski, and A. Raviv-Moshe, Phys. Rev. Lett. **128**, 021603 (2022).

[79] H. Casini, I. S. Landea, and G. Torroba, Phys. Rev. Lett. **130**, 111603 (2023).

[80] G. Cuomo, Z. Komargodski, and M. Mezei, Journal of High Energy Physics **2022**, 134 (2022), arXiv:2112.10634 [hep-th].

[81] R. Lanzetta, S. Liu, and M. Metlitski, To appear.

[82] G. Cuomo, Y. C. He, and Z. Z. Komargodski, J. High Energy Phys. **11**, 061.

[83] K. Jensen and A. O'Bannon, Phys. Rev. Lett. **116**, 091601 (2016).

[84] A. B. Zamolodchikov, JETP Letter **43**, 730 (1986).

[85] J. L. Cardy, Physics Letters B **215**, 749 (1988).

[86] Z. Komargodski and A. Schwimmer, Journal of High Energy Physics **2011**, 10.1007/jhep12(2011)099 (2011).

[87] D. L. Jafferis, I. R. Klebanov, S. S. Pufu, and B. R. Safdi, Journal of High Energy Physics **2011**, 102 (2011), arXiv:1103.1181 [hep-th].

[88] R. C. Myers and A. Sinha, Phys. Rev. D **82**, 046006 (2010), arXiv:1006.1263 [hep-th].

[89] H. Casini and M. Huerta, Phys. Rev. D **85**, 125016 (2012), arXiv:1202.5650 [hep-th].

[90] S. Banerjee, Y. Nakaguchi, and T. Nishioka, Journal of High Energy Physics **2016**, 10.1007/jhep03(2016)048 (2016).

[91] I. Klebanov, S. Pufu, and B. Safdi, Journal of High Energy Physics **2011**, 38 (2011).

[92] S. Giombi and I. R. Klebanov, Journal of High Energy Physics **2015**, 117 (2015).

[93] L. Fei, S. Giombi, I. R. Klebanov, and G. Tarnopolsky, Journal of High Energy Physics **2015**,

1–37 (2015).

[94] S. Giombi, E. Himwich, A. Katsevich, I. R. Klebanov, and Z. Sun, arXiv e-prints , arXiv:2412.14086 (2024).